AGU PUBLICATIONS

Paleoceanography and Paleoclimatology

RESEARCH ARTICLE
10.1002/2017PA003201

Key Points:
- The alkenone paleothermometer is one of the most widely used techniques for inferring past sea surface temperature
- We explore extant issues with calibration of the alkenone proxy, including seasonality and nonlinearity
- We propose a new calibration, BAYSPLINE, to infer SSTs from alkenones and show that it improves inference, especially in the tropics

Supporting Information:
- Supporting Information S1
- Data Set S1

Correspondence to:
J. E. Tierney,
jesst@email.arizona.edu

Citation:
Tierney, J. E., & Tingley, M. P. (2018). BAYSPLINE: A new calibration for the alkenone paleothermometer. *Paleoceanography and Paleoclimatology*, *33*, 281–301. https://doi.org/10.1002/2017PA003201

Received 28 JUN 2017
Accepted 22 JAN 2018
Accepted article online 6 FEB 2018
Published online 23 MAR 2018

BAYSPLINE: A New Calibration for the Alkenone Paleothermometer

Jessica E. Tierney[1] **and Martin P. Tingley**[2]

[1]Department of Geosciences, University of Arizona, Tucson, AZ, USA, [2]Department of Meteorology, Pennsylvania State University, University Park, PA, USA

Abstract The alkenone-based $U^{K'}_{37}$ proxy is a cornerstone of paleoclimatology, providing insight into the temperature history of the Earth's surface ocean. Although the relationship between $U^{K'}_{37}$ and sea surface temperatures (SSTs) is robust and well supported by experimental data, there remain outstanding issues regarding the seasonality of production of alkenones and the response of $U^{K'}_{37}$ at very warm and cold SSTs. Using a data set of over 1,300 core-top $U^{K'}_{37}$ measurements, we find compelling evidence of seasonal production in the North Atlantic, North Pacific, and Mediterranean Oceans. We also find significant attenuation of the $U^{K'}_{37}$ response to SST at warm temperatures (>24°C), with the slope reduced by nearly 50% as $U^{K'}_{37}$ approaches unity. To account for these observations in a calibration, we develop a new Bayesian B-spline regression model, BAYSPLINE, for the $U^{K'}_{37}$ paleothermometer. BAYSPLINE produces similar estimates as previous calibrations below ~24°, but above this point it predicts larger SST changes, in accordance with the attenuation of the $U^{K'}_{37}$ response. Example applications of BAYSPLINE demonstrate that its treatment of seasonality and slope attenuation improves paleoclimatic interpretations, with important consequences for the inference of SSTs in the tropical oceans. BAYSPLINE facilitates a probabilistic approach to paleoclimate, building upon growing efforts to develop more formalized statistical frameworks for paleoceanographic reconstruction.

Plain Language Summary "Alkenones" are lipids (fats) made by marine phytoplankton. The plankton alter the degree of unsaturation in these lipids in response to sea surface temperature (SST), producing more unsaturated compounds in colder water. These lipids are well preserved in marine sediments, such that paleoclimatologists can measure the unsaturation and determine what SSTs were in the past. In this manuscript, we review the calibration of this powerful "paleothermometer" and propose a new model that uses spline fits and Bayesian regression. We find that the new model improves our ability to estimate past SSTs, especially in the tropical oceans.

1. Introduction

The alkenone paleotemperature proxy is one of the most widely used methods for estimating sea surface temperatures (SSTs) in paleoceanography. The proxy is based on the relative unsaturation of long-chain (C_{37}) ketone lipids (alkenones) produced by haptophyte algae like *Emiliana huxleyi* (Brassell et al., 1986; Marlowe et al., 1984; Volkman et al., 1980). Unsaturation decreases with increasing temperature, consistent with a homeoviscous adaptation, although alkenones are presumed to be energy storage molecules and not membrane lipids (Epstein et al., 2001).

Haptophytes produce alkenones with 37, 38, and 39 carbons and all demonstrably change in response to water temperature, but the C_{37} group is traditionally targeted for paleoceanographic applications. The relative unsaturation of these compounds is represented mathematically by the U^{K}_{37} and $U^{K'}_{37}$ indices:

$$U^{K}_{37} = \frac{C_{37:2} - C_{37:4}}{C_{37:2} + C_{37:3} + C_{37:4}} \quad (1)$$

$$U^{K'}_{37} = \frac{C_{37:2}}{C_{37:2} + C_{37:3}}. \quad (2)$$

Although inclusion of the $C_{37:4}$ compound may afford some predictive benefits in cold waters (Bard, 2001; Bendle & Rosell-Melé, 2004), this compound is absent from many marine sediment profiles, simplifying U^{K}_{37} to $U^{K'}_{37}$. Here we focus exclusively on the $U^{K'}_{37}$ index, the most commonly used form in paleoceanography.

In the past 30 years, the alkenone paleothermometer has been repeatedly calibrated, validated, and examined for sensitivity to nonthermal effects such as light and nutrient stress (Prahl et al., 2003), degradation (Hoefs et al., 1998; Prahl, De Lange et al., 1989), and lateral advection (Mollenhauer et al., 2003; Rühlemann & Butzin, 2006). Although these secondary influences on $U^{K'}_{37}$ are nonnegligible in some locations, they are difficult to detect on a global scale (Herbert, 2001; 2003). Importantly, the sensitivity of $U^{K'}_{37}$ to temperature has been confirmed by laboratory culturing of *Emiliana huxleyi* and *Gephyrocapsa oceanica*, the dominant producers of alkenones in the modern ocean (Conte et al., 1998; Prahl & Wakeham, 1987; Prahl et al., 1988; Sawada et al., 1996; Volkman et al., 1995). Although some strain-dependent differences exist, these experiments generally indicate a $U^{K'}_{37}$ sensitivity close to the empirical values derived from regressing core-top $U^{K'}_{37}$ against observed SSTs (Herbert, 2001; Müller et al., 1998; Sikes et al., 1991). This agreement confirms that the alkenone paleothermometer is a robust indicator for SSTs or very near-surface (upper mixed layer) ocean temperatures.

In spite of decades of research, unanswered questions regarding calibration of the alkenone paleothermometer remain and may pose serious issues for estimation in certain regions or time periods. One concern is the relatively recent appearance of *E. huxleyi* in the fossil record (~290 ka, Raffi et al., 2006; Thierstein et al., 1977), which dominates alkenone production in the modern ocean. Likewise, the second-most important producer, *G. oceanica*, only appears in the Pliocene (present at 3.5 Ma, abundant at 1.7 Ma, Raffi et al., 2006, Samtleben, 1980). Prior to the evolution of *G. oceanica*, alkenones are still abundant in sediments but were presumably produced by now-extinct relatives (Marlowe et al., 1990). Therefore, temperature estimation before the mid-Pliocene necessarily relies on the assumption that the $U^{K'}_{37}$ sensitivity to seawater temperature is the same as today. However, a similar assumption must be made for nonextant species of planktic foraminifera (Zachos et al., 1994), so this is a common and particularly intractable problem in paleoceanography that is not unique to $U^{K'}_{37}$.

More tractable problems regarding $U^{K'}_{37}$ calibration include the seasonality of production and the potential for nonlinear temperature sensitivity at the low and high ends of the calibration range. Sediment trap studies demonstrate that alkenone production varies strongly throughout the annual cycle in most regions, with factors such as temperature, nutrients, stratification, and competition regulating the timing of haptophyte blooms (Rosell-Melé & Prahl, 2013). In the subtropics and midlatitudes, production is typically skewed toward spring, following nutrient entrainment from late winter and spring mixing (Prahl et al., 1993; Richey & Tierney, 2016). In the high latitudes, blooms occur during summer or fall as light availability and competition with other phytoplankton play a role (Rosell-Melé & Prahl, 2013; Seki et al., 2007; Sikes et al., 2005; Thomsen et al., 1998). In the Mediterranean, production occurs throughout the fall and spring and is low during the warm, stratified summer season (Ternois et al., 1996). It is still unclear how, or whether, seasonal bias in production affects sedimentary $U^{K'}_{37}$, which is typically calibrated to mean annual temperatures. Some sediment trap studies note that core-top sediments below the trap site appear to reflect annual SST in spite of seasonal variability, suggesting that there is some attenuation and averaging of the seasonal signals occurring during the export process (e.g., Müller & Fischer, 2001). Mean annual SST also appears to be a defensible choice for calibrating existing core-top data sets (Conte et al., 2006; Müller et al., 1998) suggesting that seasonal bias may not be large enough to affect alkenone signatures on a global scale. On the other hand, close investigation of residual patterns that emerge after calibrating to mean annual SST suggests that $U^{K'}_{37}$-based estimates may be seasonally biased in some regions, in particular, the high latitudes (Prahl et al., 2010; Rosell-Melé & Prahl, 2013).

The linearity of the $U^{K'}_{37}$ response to SST is also an unresolved issue. Prahl et al. (1988) cultured *E. huxleyi* at five temperatures and found that a constant slope (0.034 $U^{K'}_{37}$ units per degrees Celsius) described the relationship between $U^{K'}_{37}$ and temperature from 8°C to 25°C well. However, a study of suspended particulate matter (SPM) in the Southern Ocean indicated that the response of unsaturation to temperature is nonlinear at cold temperatures (Sikes & Volkman, 1993). A later culturing study of multiple strains of haptophytes observed slope attenuation below 12°C and above 24°C, suggesting that the temperature sensitivity of $U^{K'}_{37}$ follows a sigmoidal curve (Conte et al., 1998). Further support for slope attenuation at low and high temperatures comes from an SPM study in the North Atlantic (Sicre et al., 2002) and sediment trap studies in warm waters (Goñi et al., 2001; Richey & Tierney, 2016), which observed clear reductions in the sensitivity of $U^{K'}_{37}$ to SST at temperatures below 6°C and above 24°C, respectively. As is the case with seasonality of production, it is unclear how much these observations of nonlinearity affect the global calibration of $U^{K'}_{37}$. Existing core-top calibrations have found that a constant slope fits the data sufficiently (Conte et al., 2006; Müller et al., 1998; Sikes et al., 1991), and some argue that "warm end" attenuation is small and/or not statistically significant

(Kienast et al., 2012; Pelejero & Grimalt, 1997). However, Conte et al. (2006) proposed a nonlinear calibration for a global $U^{K'}_{37}$ SPM data set, and Sonzogni et al. (1997) proposed a reduced slope (0.023) for $U^{K'}_{37}$ calibration in the tropical Indian Ocean.

In what follows, we first reexamine the alkenone paleothermometer with an extended and updated core-top data set, with an emphasis on resolving issues regarding seasonality and nonlinearity. Next, we introduce a Bayesian $U^{K'}_{37}$ calibration model that addresses attenuation at high SSTs and provides a probabilistic method for propagating uncertainties in the $U^{K'}_{37}$ calibration through to paleoclimatic reconstruction—an aspect critical for multiproxy inference, model-data comparisons, and data assimilation (e.g., Annan & Hargreaves, 2013; Steiger & Hakim, 2016; Tingley et al., 2012). We then assess the performance of this new calibration by applying it to published $U^{K'}_{37}$ records and comparing results with previous calibrations as well as independent proxies for SST. Finally, we discuss how our new $U^{K'}_{37}$ calibration affects paleoceanographic interpretations, particularly in the tropical oceans.

2. Data Compilation and Analytical Methods

2.1. $U^{K'}_{37}$ and SST Data

We compiled core-top $U^{K'}_{37}$ data from previous global calibration efforts (Conte et al., 2006; Müller et al., 1998), regional studies of $U^{K'}_{37}$ patterns (Benthien & Müller, 2000; Cacho, Pelejero et al., 1999; Chen et al., 2014; Doose et al., 1997; dos Santos et al., 2010; Fallet et al., 2012; Filippova et al., 2016; Herbert et al., 1998; Ho et al., 2012; Jaeschke et al., 2017; Kaiser et al., 2014; Kienast et al., 2012; Kim et al., 2015; Leduc et al., 2010; Lee, Kim et al., 2008; Leider et al., 2010; Madureira et al., 1995; Mohtadi et al., 2011; Ohkouchi et al., 1999; Pelejero & Grimalt, 1997; Prahl et al., 2006, 2010; Rodrigo-Gámiz et al., 2015; Rosell-Melé et al., 1995, 2000; Rosell-Melé, 1998; Sawada et al., 1996; Sikes et al., 1991, 1997; Sonzogni et al., 1997; Tao et al., 2012), and Late Quaternary studies where a modern or latest Holocene core top was measured (Arz et al., 2003; Bard et al., 2000; Barron et al., 2003; Barrows et al., 2007; Becker et al., 2015; Bendle & Rosell-Melé, 2007; Budziak et al., 2000; Cacho, Grimalt et al., 1999; Cacho et al., 2001; Calvo et al., 2001, 2007; Caniupán et al., 2011; Chapman et al., 1996; Dubois et al., 2009; Emeis et al., 2000, 2003; Fraser et al., 2014; Gutiérrez et al., 2011; Harada et al., 2006; Herbert et al., 2001; Horikawa et al., 2006; Huang et al., 1997; Ikehara et al., 1997; Jaeschke et al., 2007; Kaiser et al., 2005, 2008; Kennedy & Brassell, 1992; Kienast & McKay, 2001; Kienast et al., 2006; Kim, Schneider, Hebbeln et al., 2002; Kim, Schneider, Müller, & Wefer, 2002; Kim et al., 2003, 2004, 2007; Koutavas & Sachs, 2008; Kudrass et al., 2001; Lamy et al., 2002; Leduc et al., 2007; Lee et al., 2001; Lee, Bahk, & Choi, 2008; Liu & Herbert, 2004; Lückge et al., 2009; Marchal et al., 2002; Martrat et al., 2007; Max et al., 2012; McCaffrey et al., 1990; Ostertag-Henning & Stax, 2000; Pahnke & Sachs, 2006; Pahnke et al., 2007; Pailler & Bard, 2002; Pelejero et al., 1999; Prahl, Muehlhausen, & Lyle, 1989; Rein et al., 2005; Rodrigues et al., 2009, 2010; Romero et al., 2008; Rühlemann et al., 1999; Sachs, 2007; Sawada & Handa, 1998; Schefuß et al., 2005; Schulz et al., 2002; Seki et al., 2004; Sepúlveda et al., 2009; Sperling et al., 2003; Sikes & Keigwin, 1994, 1996; Sikes et al., 2009; Sonzogni et al., 1998; Ternois et al., 2000; Weldeab et al., 2007; Zhao et al., 1995, 2006). We also analyzed $U^{K'}_{37}$ in 132 additional core tops to increase spatial coverage. The complete core-top data set is available as a Data Set S1 in the supporting information. The laboratory methodology for the new analyses is described in the subsequent subsection. In total, our compilation contains 1,344 core tops distributed across the modern ocean (Figure 1). $U^{K'}_{37}$ values in the core-top data set span 0.033–1, covering nearly all of the possible range (0–1). A $U^{K'}_{37}$ value of 1 indicates that the $C_{37:3}$ compound is undetectable via conventional gas chromatographic techniques and therefore is assigned a peak area of zero. Some have argued that $U^{K'}_{37}$ values of 1 be excluded from calibration exercises because there is both technical and interpretive ambiguity in the assignment of a value of zero to $C_{37:3}$ (Pelejero & Calvo, 2003). However, our opinion is that these values must be retained, because they represent a source of user error and interpretation that we seek to capture in our assessment of error variance. Practically speaking, there are only 19 values in our data set with $U^{K'}_{37}$=1, and so their inclusion has a negligible impact on our results (inferred regression coefficients differ by a maximum of 5%).

To calibrate the $U^{K'}_{37}$ data, we use instrumental SST observations from the 0.25° National Oceanic and Atmospheric Administration (NOAA) Optimum Interpolation Sea Surface Temperature (OISST) gridded product, based on a combination of ship, buoy, and satellite (advanced very high resolution radiometer) observations (Banzon et al., 2016). This product provides daily SSTs from 1981 to present. We chose OISST due to its superior coverage near the coastlines, where many of the $U^{K'}_{37}$ core tops are found (Figure 1). Our results are not sensitive to this choice of SST product; regression coefficients and predicted SSTs using the 1° World Ocean Atlas 13 data product (Locarnini et al., 2013) are virtually identical (not shown). For our purposes, we use the mean

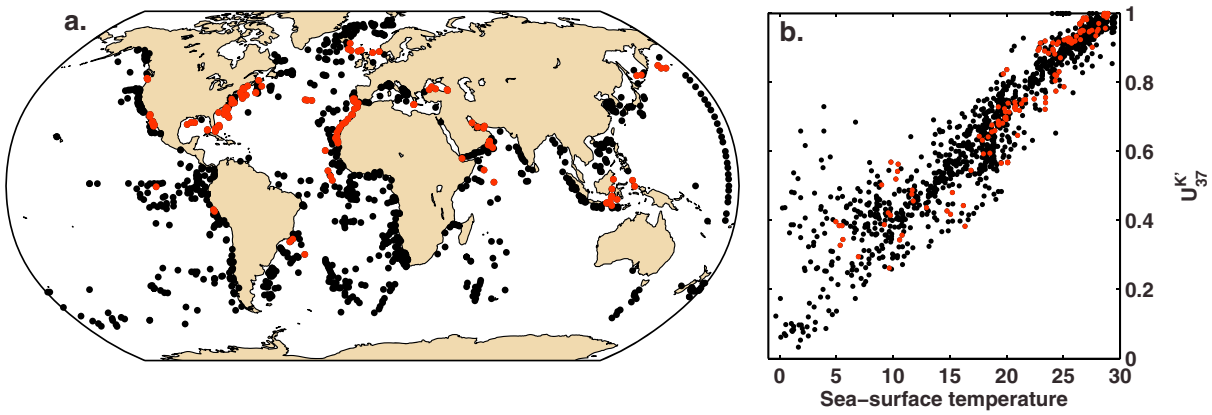

Figure 1. (a) Locations of the core-top samples in the alkenone calibration database ($N = 1344$). (b) Core-top $U^{K'}_{37}$ values versus observed sea surface temperature (Optimum Interpolation Sea Surface Temperature, Banzon et al., 2016). Red points denote new data generated as a part of this study ($N = 132$).

annual and monthly climatologies of the OISST product. Estimated standard errors for the OISST climatologies are small (fractions of a degree) so are not explicitly included in our analysis. SST and $U^{K'}_{37}$ observations are paired using minimum chordal distances (after Tierney & Tingley, 2014). The $U^{K'}_{37}$ data sample a wide range of modern SSTs from −0.4 to 29.6°C (Figure 1).

Prior to calculating any correlations or regressions, paired $U^{K'}_{37}$-SST values from the anomalous Brazil-Malvinas and Arctic regions were removed (see sections 3 and 4 below) and $U^{K'}_{37}$ values from the same OISST grid point were averaged to avoid spatial overrepresentation. This results in an effective core top $N = 1137$.

2.2. Analytical Methods for New $U^{K'}_{37}$ Core Tops

We sampled 1–2 cm of sedimentary material from the top (e.g., 0–1 and 0–2) or, if upper sediments were unavailable, the near top (in most cases, upper 10 cm) of 132 sediment cores stored at the Woods Hole Oceanographic Institution Seafloor Samples Repository. The 123 of 132 of these cores were box cores, multicores, or gravity cores, ensuring that the uppermost sediment is most likely recent (e.g., late Holocene) in age. Many of these sediments were subject to investigation in other core-top-based studies, verifying their utility for modern calibration study (e.g., Dekens et al., 2002; Lear et al., 2002). The remaining 10 samples were piston cores, where loss of the uppermost sediment due to the coring process is likely. To mitigate the possibility of sampling old (in particular, glacial) sediments, we specifically targeted piston cores that had confirmed Holocene sediments from previous investigations in the published literature. Thus, we are confident that our core-top sediments are at least Holocene in age, during which time temperature variations were minimal relative to the range of the calibration data set (i.e., on the order of a couple of degrees). It should be noted that the problem of "ambiguous modernity" afflicts the entire core-top $U^{K'}_{37}$ data set and that we do not have specific information regarding the age of each core top. This uncertainty undoubtedly contributes to the error variance of the calibration.

Sediment samples were freeze-dried and homogenized, and then ~5–10 g of material was extracted with an accelerated solvent extraction 350 system at a temperature of 100°C and maximum pressure of 10,342 kPa. If necessary, the resulting total lipid extracts (TLEs) were run through a short column of sodium sulfate to remove any interstitial seawater released during the extraction process. TLEs were then evaporated to dryness and purified using two column chromatography steps. First, neutral, acid, and polar fractions were separated over LC-NH_2 gel using dichloromethane:isopropanol (2:1), 4% acetic acid in dichloromethane, and methanol as the respective eluents. Next, the neutral and polar fractions were recombined, then further purified over 5% deactivated silica gel using hexane, dichloromethane, and methanol as eluents. The dichloromethane fraction, containing the alkenones, was redissolved in ethyl acetate in preparation for analysis by gas chromatography.

Alkenones were detected and quantified on a Trace 1310 gas chromatograph equipped with a DB-1 column (60 m × 0.32 mm × 0.1 μm) and a programmable temperature vaporization (PTV) injector. The PTV was operated in splitless mode (splitless time: 3 min) with a program of: 60°C (held 0.1 min) to 325°C at 5°C/s, and a ramped pressure from 14.5 psi to 33.6 psi. The gas chromatograph oven program (total runtime: 70 min) was: 60°C (held 2 min) to 270°C at 30°C/min, then to 310°C at 1°C/min (hold 1 min), then to 325°C at 10°C/min (hold 18.50 min). Alkenones were identified via comparison of retention times to internal laboratory standards.

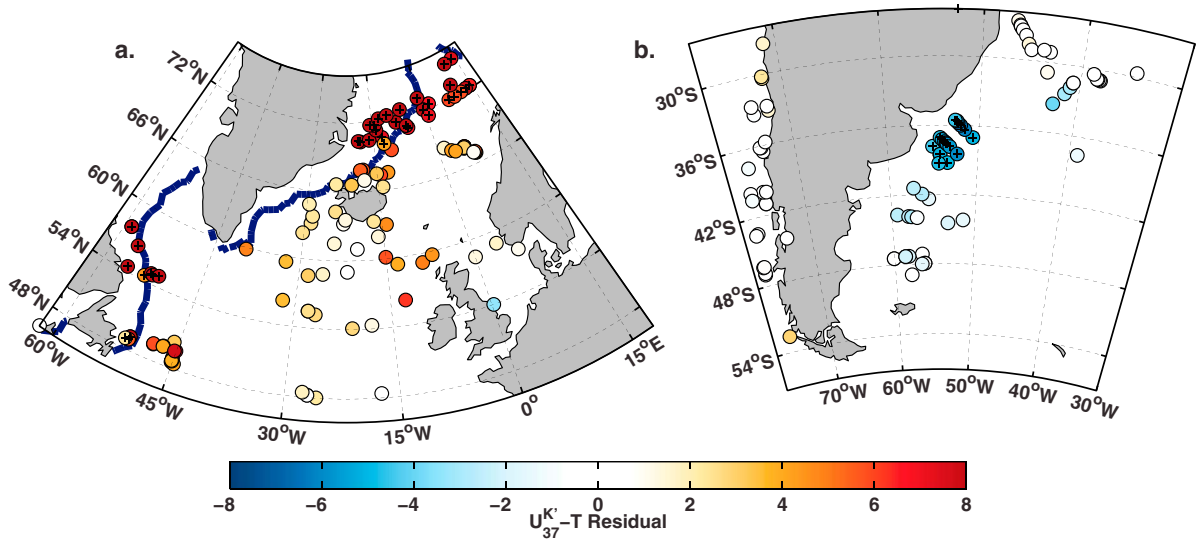

Figure 2. Locations with large $U^{K'}_{37}$ residuals (observed $U^{K'}_{37}$- predicted $U^{K'}_{37}$, converted to temperature units by dividing by the slope) when applying the Prahl et al. (1988) calibration. (a) $U^{K'}_{37}$ residuals in the North Atlantic region. Note high values in the Nordic Seas and Labrador Sea. Dark blue line encloses regions with at least 5% annual sea ice cover. (b) $U^{K'}_{37}$ residuals in the Brazil-Malvinas confluence region. Core tops marked with plus signs were excluded from further calibration exercises (see text).

Quantification was achieved via comparison of the alkenone peak areas to the peak area of a known amount of stearyl stearate, which was added to the TLE of each sample after accelerated solvent extraction. The $U^{K'}_{37}$ index was calculated according to equation (1). The precision (1σ) of the $U^{K'}_{37}$ values was 0.002 units based on repeat measurements of a laboratory sediment standard.

3. Data Exploration: Residual Trends, Seasonality, and Nonlinearity

To investigate spatially varying trends in the $U^{K'}_{37}$-temperature response, we applied the linear culture calibration of Prahl et al. (1988) ($U^{K'}_{37} = 0.034 \cdot T + 0.039$, with T = mean annual SST), to the calibration data set and examined the residuals. We choose this calibration as our baseline for comparison because it (1) is "theoretical" in the sense that is based on controlled laboratory cultures, (2) was explicitly recommended for paleoceanographic application by the alkenone community in 2000 (Prahl et al., 2000), and (3) is not significantly different from the core-top-based calibration of Müller et al. (1998), which is commonly applied to $U^{K'}_{37}$ data. Thus, we can consider areas of large residual values as regions where $U^{K'}_{37}$ behavior deviates from this theoretical expectation.

In the current data set, there are three areas with very large (~5°C) residuals: the Nordic Seas, the Labrador Sea, and a small zone at the confluence of the Brazil and Malvinas currents (Figure 2). Previous studies have identified these regions as problematic for alkenone paleothermometry (Bendle & Rosell-Melé, 2004; Benthien & Müller, 2000; Conte et al., 2006; Filippova et al., 2016; Rühlemann & Butzin, 2006). The anomalously low $U^{K'}_{37}$ values in the Brazil-Malvinas region are attributed to lateral advection of alkenones generated in the cold waters south of the front (Benthien & Müller, 2000; Conte et al., 2006; Rühlemann & Butzin, 2006). Likewise, the anomalously high $U^{K'}_{37}$ values found in the Nordic and Labrador Seas are located near frontal SST boundaries and thus could indicate lateral advection of alkenones from warmer waters to the south (Bendle & Rosell-Melé, 2004). However, the absolute $U^{K'}_{37}$ values at some of these locations are similar to those found in subtropical waters (~0.5–0.7), indicating either very far field advection or that another process is influencing alkenone unsaturation. Filippova et al. (2016) observed that although sea ice intensity is not correlated with $U^{K'}_{37}$ residuals in the high-latitude North Atlantic, nearly all of the samples with higher $U^{K'}_{37}$ values than expected are from locations with some sea ice cover. Indeed, we find that the most positive residuals in the Norwegian and Labrador Seas generally, although not exclusively, fall within areas with at least 5% annual ice cover (Figure 2a) and that there is a significant correlation between $U^{K'}_{37}$ residuals and the percentage of annual sea ice cover (Spearman's $\rho = 0.52$, $p < 0.0001$). This suggests an unknown ecophysiological impact on alkenone unsaturation in areas with seasonal sea ice.

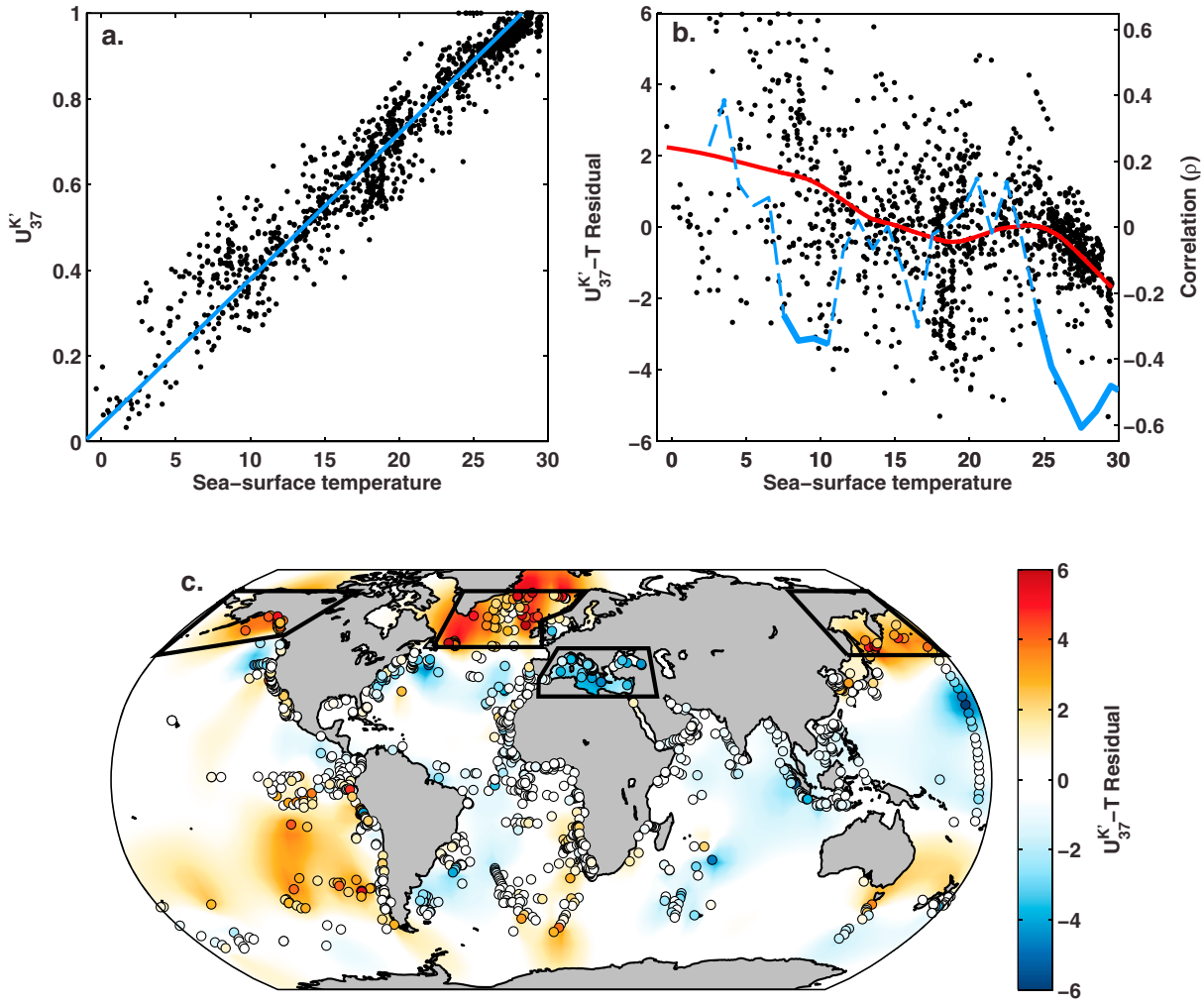

Figure 3. (a) Core-top $U^{K'}_{37}$ versus sea surface temperature with points marked in Figure 2 removed. Blue line denotes the Prahl et al. (1988) regression. (b) $U^{K'}_{37}$ residuals (observed $U^{K'}_{37}$-predicted $U^{K'}_{37}$, converted to temperature units by dividing by the slope) when applying the Prahl et al. (1988) calibration. Red line represents a locally weighted scatterplot smoothing of the data with a span of 40% to highlight trends in the residuals. Blue line shows running Spearman correlation (ρ) values for 5° moving windows (plotted at the midpoint of the windows, axis on right). Solid blue line indicates significant correlations ($p < 0.05$). (c) Global distribution of $U^{K'}_{37}$ residuals. Ordinary kriging is used to interpolate between individual data points for visualization purposes. Black boxes enclose areas with a seasonal $U^{K'}_{37}$ bias, further explored in Figure 4.

Given that these unusual $U^{K'}_{37}$ values would heavily skew a regression, following previous work (Conte et al., 2006), we omit the data from the Brazil-Malvinas region and the Nordic and Labrador Seas (in the Nordic Seas, points north of 70°N; in the Labrador Sea, points west of 50°W) from further calibration exercises (Figure 2). In doing so, we preclude the application of the alkenone paleothermometer in these regions. Although alternate alkenone indices show some promise in the Nordic Seas (Bendle & Rosell-Melé, 2004; Rosell-Melé, 1998), our concern here is with $U^{K'}_{37}$, which interestingly, like the other lipid-based paleothermometer TEX_{86}, fails to reflect temperatures in the cold, high-latitude Arctic (Ho et al., 2014; Kim et al., 2010; Tierney & Tingley, 2014). As with TEX_{86}, $U^{K'}_{37}$ performs adequately in the cold Southern Ocean, suggesting that this is not a thermal limitation of the proxy but rather the presence of confounding influences in the Arctic region.

With the data from the Brazil-Malvinas confluence and Arctic regions removed, global residuals calculated from the Prahl et al. (1988) calibration are much more uniform, but there are still regions and temperatures for which distinct patterns can be observed (Figure 3). In particular, both the North Atlantic and North Pacific regions have positive residuals, resulting in a significant negative correlation between residual $U^{K'}_{37}$ and temperature between ~7 and 10°C (Figure 3b). It is also clear that core tops in the Mediterranean and Black Sea have consistently lower $U^{K'}_{37}$ than expected (Figure 3c). $U^{K'}_{37}$ in the southeast Pacific is anomalously high

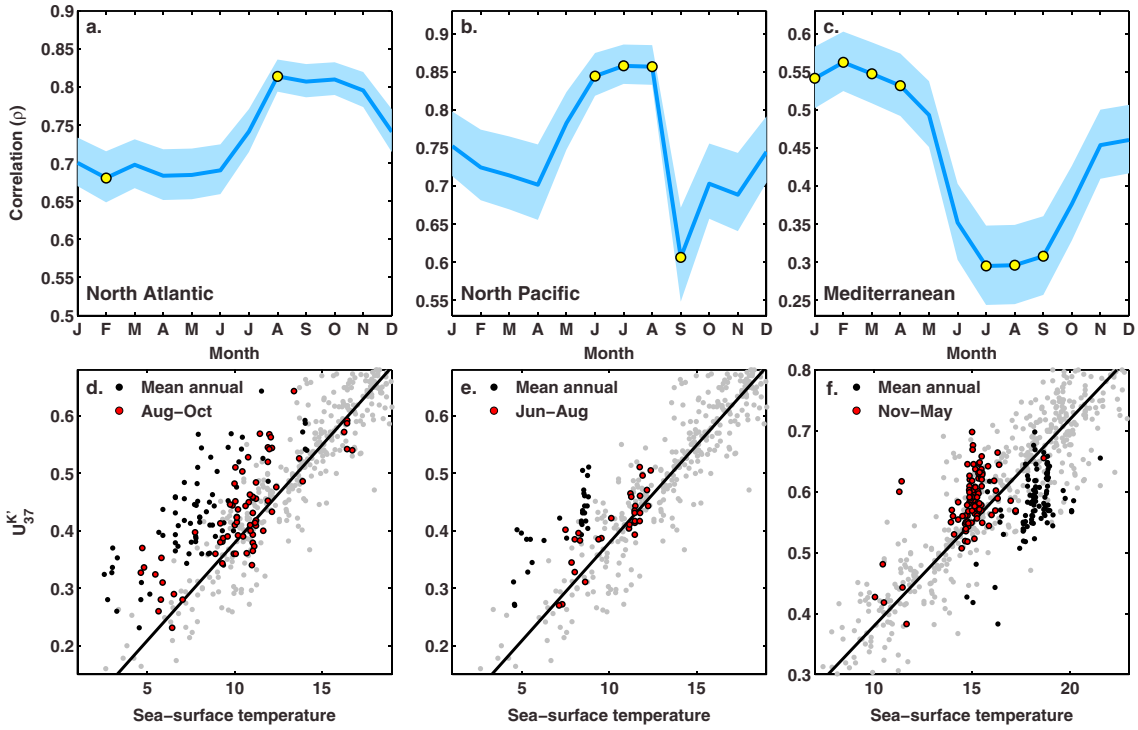

Figure 4. (a–c) Monthly correlations (Spearman's ρ) between sea surface temperatures (SSTs) and $U^{K'}_{37}$ core tops in the North Atlantic (area north of 48°N excluding the Labrador and North Seas); North Pacific (area north of 45°N in the western region and 52.5°N in the eastern region), and Mediterranean (including the Black Sea), respectively. See Figure 3c for a map of the highlighted areas. Yellow dots denote maximum and minimum correlations with a low probability ($p < 0.10$) of being statistically indistinguishable. Error bars represent the 1σ uncertainty on the correlation value. (d–f) Core-top data from each region calibrated to mean annual SST (in black) versus seasonal SSTs (in red) where maximum correlations in Figures 4a–4c are found. Other data from the core-top data set are plotted in gray, and the black line denotes the Prahl et al. (1988) regression.

(Figure 3c). Finally, while not visually apparent in the spatial distribution of residuals (Figure 3c), there is a strong negative correlation between residual $U^{K'}_{37}$ and SST above 24°C (Figure 3b).

The residual patterns in the northern latitudes and the Mediterranean may be expressions of a seasonal influence on core-top $U^{K'}_{37}$. These regions experience a large range of SSTs through the annual cycle (4–14°C), and haptophyte blooms tend to be seasonally restricted (Rosell-Melé & Prahl, 2013; Seki et al., 2007; Ternois et al., 1997; Thomsen et al., 1998). Thus, the potential for a seasonal bias in sedimentary $U^{K'}_{37}$ is high. To empirically assess seasonal bias in these areas, we investigated month-by-month correlations between regional $U^{K'}_{37}$ and SSTs (Figures 4a–4c). For all three regions, there is a clear seasonal pattern in correlation, with a low probability that maximum and minimum correlation values are the same (Figures 4a–4c). For the North Atlantic and North Pacific, the data suggest that core-top $U^{K'}_{37}$ best reflects SSTs from August–October and June–August, respectively (Figures 4a and 4b). This empirical finding largely agrees with sediment trap evidence of alkenone production patterns in these regions, which indicate maximum flux during summer and fall (Rosell-Melé & Prahl, 2013; Seki et al., 2007; Thomsen et al., 1998).

The Mediterranean $U^{K'}_{37}$ data have high correlations with November–May SSTs (Figure 4c), in agreement with sediment trap data that indicate maximum alkenone flux in fall and spring (Ternois et al., 1997). However, changes in the depth of production may also be a factor; in a study of upper water column SPM from the northwestern Mediterranean, Ternois et al. (1996) observed maximum alkenone concentrations from 20 to 50 m during fall and spring but from 50 to 70 m during the summer months, which is at or just below the shallow thermocline. A cooler summer signal combined with a upper mixed layer signal from the winter months would result in lower-than-expected sedimentary $U^{K'}_{37}$. To investigate whether calibration to deeper-water temperatures could explain the Mediterranean $U^{K'}_{37}$ distributions, we compared $U^{K'}_{37}$ values to mean annual temperatures from different depths, derived from the World Ocean Atlas 2013 product (Locarnini et al., 2013). We found that maximum correlations occurred when $U^{K'}_{37}$ was regressed against temperatures from 65 to 100 m depth (not shown); however, the value ($\rho = 0.68$) was not statistically different from the correlation

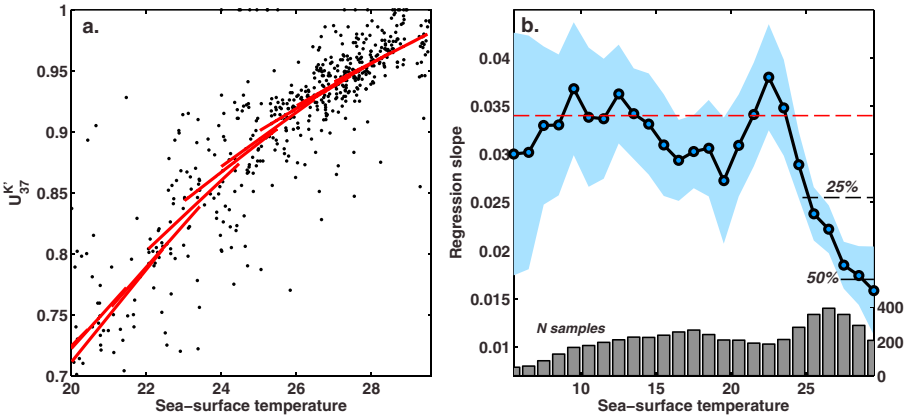

Figure 5. (a) Piecewise regression lines (in red) reveal slope attenuation in the core-top data set (black dots) above about 24°C. (b) Piecewise regression slope plotted as a function of sea surface temperature (midpoint of regression bin). Dots represent mean values; blue shading represents the 95% confidence interval. Red dotted line represents the Prahl et al. (1988) slope. Gray bars at bottom show the number of core-top data in each bin (*N* samples). The black dotted lines show the point at which the slope reaches 25% and 50% attenuation of the Prahl value (0.034).

with SSTs ($\rho = 0.56$, $p = 0.53$). Therefore, from an empirical perspective winter-spring production is the best explanation for the negative $U^{K'}_{37}$ residuals in the Mediterranean.

The southeast Pacific core-top data also show consistently high $U^{K'}_{37}$ residuals (Figure 3c); however, the authors of the study from which these data derive suspect preferential degradation of the $C_{37:3}$ in this region (leading to artifically high $U^{K'}_{37}$), as alkenone concentrations are low and there is independent biomarker evidence for extensive sedimentary organic matter degradation (Jaeschke et al., 2017). Our analysis supports a nonseasonal origin for a $U^{K'}_{37}$ bias in this region, as we do not observe increases in correlation by month or season (not shown). We also note the large negative residuals in the North Pacific (Figure 3c). This feature is also likely to have a sedimentary, rather than seasonal origin: sedimentation rates are very low at this location (on the order of millimeters per kiloannum), and thus, glacial (cooler) alkenones could have been mixed into the core-top samples.

The negative trend in residuals above ~24°C suggests a nonlinear response of $U^{K'}_{37}$ to temperature above this threshold. As discussed in section 1, nonlinearity at the high end of the $U^{K'}_{37}$ calibration has long been suspected and is evident in water column and sediment trap studies (Goñi et al., 2001; Richey & Tierney, 2016; Sikes & Volkman, 1993). To more directly assess whether the global core-top data set shows evidence of slope attenuation, we conducted piecewise regression in 5°C bins spanning 3–30°C (data between 0 and 3°C were excluded due to the low number of core-top samples). In agreement with the pattern in the residuals, slope attenuation is visually apparent above 24°C (Figure 5a). While the slope remains within uncertainty of the Prahl culture expectation between 3 and 23°C, it drops sharply at higher temperatures, reaching a 25% reduction around 25° and 50% reduction around 27° (Figure 5b). This slope reduction is statistically significant ($p < 0.05$) from 24° upward. Large *N* at the high end of the calibration range gives confidence in the regression coefficients and confirms that this attenuation is not an artifact of data availability (Figure 5b). Interestingly, we find no evidence of significant slope attenuation at the low end of the calibration, in spite of the fact that reduced sensitivity may be expected from culture results (Conte et al., 1998) as well as analyses of SPM (Conte et al., 2006; Sikes & Volkman, 1993). However, there are a limited number of core tops available between 0 and 5° (outside of the "sea ice zone," $N = 34$) leading to large uncertainty in determination of the regression coefficients in our lowest bin of 3–8° (Figure 5b). Thus, it is possible that current sampling of cold water locations is not sufficient to detect slope attenuation.

4. BAYSPLINE: A New Calibration Model

4.1. Statistical Approach

Our analysis of the core-top data set demonstrates that $U^{K'}_{37}$ is seasonally biased in the northern high latitudes and the Mediterranean and that $U^{K'}_{37}$ sensitivity to temperature decreases substantially above 24°C. A calibration model must therefore accommodate these observations. To resolve the seasonality issue, we simply match core-top $U^{K'}_{37}$ within the regions identified in Figure 3c to seasonal temperatures inferred from our

correlations (Figure 4). This corresponds to August–October SSTs for the North Atlantic, June–August SSTs for the North Pacific, and November–May SSTs for the Mediterranean. In doing so, we make explicit in the model that temperatures inferred for these regions will correspond to a seasonal, and not annual, average.

The slope attenuation at the high end of the $U_{37}^{K'}$-SST relationship calls for a model that is flexible enough to account for nonlinearities. We experimented with sigmoidal functions, including logistic curves and Richard's curves, but these failed to adequately fit the data, resulting in further trends in the residuals (not shown). We therefore chose to use B (Basis)-splines to model the $U_{37}^{K'}$-SST relationship. B-splines have an advantageous property in that they can be linearly combined to form a spline curve (piecewise polynomial function) that can accommodate both the relatively linear relationship between $U_{37}^{K'}$ and SST below 24°C, as well as the nonlinear slope attenuation above that point. The B-spline function transforms the SST data (x) such that

$$S_n(x) = \sum_i \beta_i B_{i,n}(x), \tag{3}$$

where n is the order of the spline, i is the number of basis splines, β_i is the coefficient for each basis spline, and $B_{i,n}(x)$ is the spline evaluation of SSTs for each basis spline of order n. Knots define the breakpoints between which different basis spline functions are used, and the functions are continuous and differentiable between and at the knots. To guard against overfitting, our approach to order and knot selection is conservative; we seek the minimum order and number of knots to preserve linearity at lower temperatures (which the data support; Figure 5b) while eliminating the residual trend at the warm end of the calibration. We found that a low-order ($n = 3$) spline with three knots, one at the lowest and highest SSTs observed in the calibration data set and a third placed near the start of the attenuation (knots = [−0.4 23.6 29.6]), contains the minimum number of regression coefficients (four) sufficient to meet these stipulations. Greater complexity, that is, higher-order splines and additional knots, offered no benefits in terms of fit, while reduced complexity failed to adequately account for the nonlinearity at high SSTs.

Since our spline transformation is simply a linear combination of B-splines, the regression model conveniently becomes a multiple linear regression:

$$\begin{aligned} \mathbf{Y} &= \{B(\mathbf{X})\} \cdot \boldsymbol{\beta} + \boldsymbol{\epsilon}, \\ \boldsymbol{\epsilon} &\sim \mathcal{N}(\mathbf{0}, \tau^2 \mathrm{I}), \end{aligned} \tag{4}$$

where $\mathbf{Y}$ is the $N \times 1$ vector of $U_{37}^{K'}$ observations, $\{B(\mathbf{X})\}$ is the $N \times M$ design matrix, with each column composed of one of the basis functions evaluated at the SST values, $\boldsymbol{\beta}$ is the $M \times 1$ vector of the B-spline coefficients, and $\boldsymbol{\epsilon}$ is the $N \times 1$ vector of residual errors, approximated as a Normal distribution with a mean of 0 and variance τ^2 (multiplied by the identity matrix I).

To infer the coefficients $\boldsymbol{\beta}$ and variance τ^2 from the core-top data set, we use Bayesian inference (Gelman et al., 2003). The advantage of Bayesian inference is that uncertainties for each of our model parameters can be estimated in an ensemble-based way. The model parameter uncertainties may then be propagated when the calibration is applied to predict SSTs from downcore $U_{37}^{K'}$ values.

Generally speaking, Bayes' rule states that the posterior probability of an event is contingent upon both the likelihood and prior knowledge about event. For our application, this is written as follows:

$$p(\boldsymbol{\beta}, \tau^2 | \mathbf{Y}, \{B(\mathbf{X})\}) \propto p(\mathbf{Y} | \{B(\mathbf{X})\}, \boldsymbol{\beta}, \tau^2) \cdot p(\boldsymbol{\beta}, \tau^2). \tag{5}$$

The conditional probability on the left-hand side is what we would like to estimate: the posterior probability distribution of the regression parameters $\boldsymbol{\beta}$ and τ^2, given the calibration data and the model. This posterior is proportional to the quantity on the right-hand side: the likelihood of the $U_{37}^{K'}$ observations given the spline-transformed SST values and the regression parameters ($p(\mathbf{Y} | \{B(\mathbf{X})\}, \boldsymbol{\beta}, \tau^2)$), times a prior probability distribution $p(\boldsymbol{\beta}, \tau^2)$. The priors represent "prior knowledge" on the parameters of interest (the regression coefficients $\boldsymbol{\beta}$ and the error variance τ^2); for example, one could build in restrictions on the direction or magnitude of the parameters if it were appropriate for the system. In our case, we would like the core-top calibration data (expressed within the likelihood) to dominate the posterior, so we set our priors to be relatively "uninformative," that is, with a large standard deviation. The means for the prior distributions are derived from an ordinary least squares estimate (see Appendix A).

As the model combines a B-spline fit with Bayesian inference, we call it "BAYSPLINE." To infer the posterior, we calculate conditional posteriors and use a Gibbs sampler (Gelman et al., 2003) (see Appendix A for details).

BAYSPLINE models $U^{K'}_{37}$ as a function of the B-spline-transformed SSTs. In order to use BAYSPLINE for paleoclimate prediction—that is, predict SSTs from $U^{K'}_{37}$—we must invert the model relationship, which requires another application of Bayes' rule. The posterior distribution of SSTs ($\mathbf{X}_{new}$) is estimated from the likelihood of the $U^{K'}_{37}$ values ($\mathbf{Y}_{new}$) given the calibration model, times a prior distribution of SSTs:

$$p(\mathbf{X}_{new}|\mathbf{Y}_{new}) \propto p(\mathbf{Y}_{new}|\{B(\mathbf{X})\}, \boldsymbol{\beta}, \tau^2) \cdot p(\mathbf{X}_{new}). \quad (6)$$

Note that the uncertainties in the calibration model parameters ($\boldsymbol{\beta}, \tau^2$) are propagated through to the calculation of the posterior SSTs. A prior distribution of SSTs $p(\mathbf{X}_{new})$ is also required here for Bayesian closure. For computational convenience, we choose a Normal prior with the mean value drawn from the median Prahl et al. (1988) approximation of SST from the target $U^{K'}_{37}$ data (P_m = median $\left((\mathbf{Y}_{new} - 0.039)/0.034\right)$) and a standard deviation that is user defined. We recommend using a conservative value such as 10°C; however, the user could, for example, restrict the probability of unrealistically high or low SSTs if they have prior geological knowledge to motivate that decision. This flexibility is one of the advantages of the Bayesian approach. Due to the spline transformation, the posterior distribution does not have an analytic solution, so to carry out this inference we make use of the Metropolis algorithm (Gelman et al., 2003). See Appendix A for computational details.

4.2. Model Results

Figure 6 shows the BAYSPLINE model and its residual patterns. Although localized areas of elevated residuals are still present, the high latitudes and Mediterranean no longer exhibit a consistent pattern (Figure 6c) and there are no significant trends in the residuals (Figure 6b). The slope attenuation at warm SSTs is well described by BAYSPLINE; the trend evident in Figure 3b is absent (Figure 6b). The slope of BAYSPLINE is indistinguishable from that of Prahl et al. (1988) and other previous global calibrations below 23.4°C (0.034; see Table 1); above this point, it declines steadily to a minimum of 0.011 at the highest temperature in the calibration data set (29.4°C). The average standard (1σ) error ($\sqrt{\tau^2}$) of the BAYSPLINE model is 0.049 $U^{K'}_{37}$ units, which translates to 1.4 °C below 23.4°C and climbs to a maximum of 4.4°C for temperatures above that point (Table 1). The increase in error at high temperatures is expected, as the slope, and therefore the sensitivity of $U^{K'}_{37}$ to temperature change, declines. The error of the BAYSPLINE calibration is higher than the Prahl et al. (1988) regression, but the latter was based on only five data points from a culture experiment and does not sample core-top variance (Table 1). BAYSPLINE's error in the linear part of the spline is generally comparable to other global, core-top calibrations (Conte et al., 2006; Müller et al., 1998) who have 1σ errors between 1 and 1.5°C (Table 1).

To compare the predictive performance of BAYSPLINE with previous $U^{K'}_{37}$ calibrations, we apply the model to representative Last Glacial Maximum (LGM; 19–23 ka) to present time series that together span a wide range of $U^{K'}_{37}$ values (Figure 7). We test different prior standard deviations to assess the impact of this choice—which is user defined—on model results. Data from the Gulf of Aden (Tierney et al., 2016) traverse the warmer end of the calibration and demonstrate the effect that BAYSPLINE's treatment of slope attenuation has on inference. At this site, the Prahl et al. (1988) regression predicts Holocene SSTs that are slightly cooler than modern values (Figure 7a), and a relatively small LGM cooling of −1.8°C. The Sonzogni et al. (1997) regression, which was developed for application in the tropical Indian Ocean and has a lower slope (0.023) predicts SSTs close to modern values during the Holocene and a more generous glacial cooling of −2.6°C (Figure 7a). With a narrow prior standard deviation of 5°C, BAYSPLINE produces a similar cooling (−2.5°C), only with slightly warmer median temperatures (Figure 7a). With more generous priors, BAYSPLINE predicts temperatures during the Holocene (~29–30°C) that are on average warmer than modern SSTs (but overlap within uncertainties) and a greater magnitude of glacial cooling (−2.9 to −3.5°C; Figure 7a). Although glacial SSTs inferred by BAYSPLINE vary little given different prior standard deviations, there is a larger spread (~1°C) during the Holocene period (Figure 7a). This reflects increased sensitivity to the prior as the $U^{K'}_{37}$ values (0.97–0.99) approach the limit of the proxy. At these high values, the slope is low (~0.015 or less), there is greater uncertainty in its determination, the likelihood of SSTs becomes expanded, and therefore the Bayesian inference relies more heavily on the relatively uninformative prior. Arguably, some constraint from the prior is needed to exclude SST values that are clearly unrealistic, for example, 40–50°C. However, a prior that is too narrow (5°C in this case) artificially restricts the glacial-interglacial range. A balance is struck with a prior standard deviation of 10°C, under which extreme temperatures (>40°C) have an appropriately low probability (<5%). With this prior assumption, median LGM cooling at the Gulf of Aden site is −3.2°, a magnitude that is in good agreement with independent, Mg/Ca-based estimates from the Arabian Sea region (Dahl & Oppo, 2006; Saraswat et al., 2013; Tierney et al., 2016).

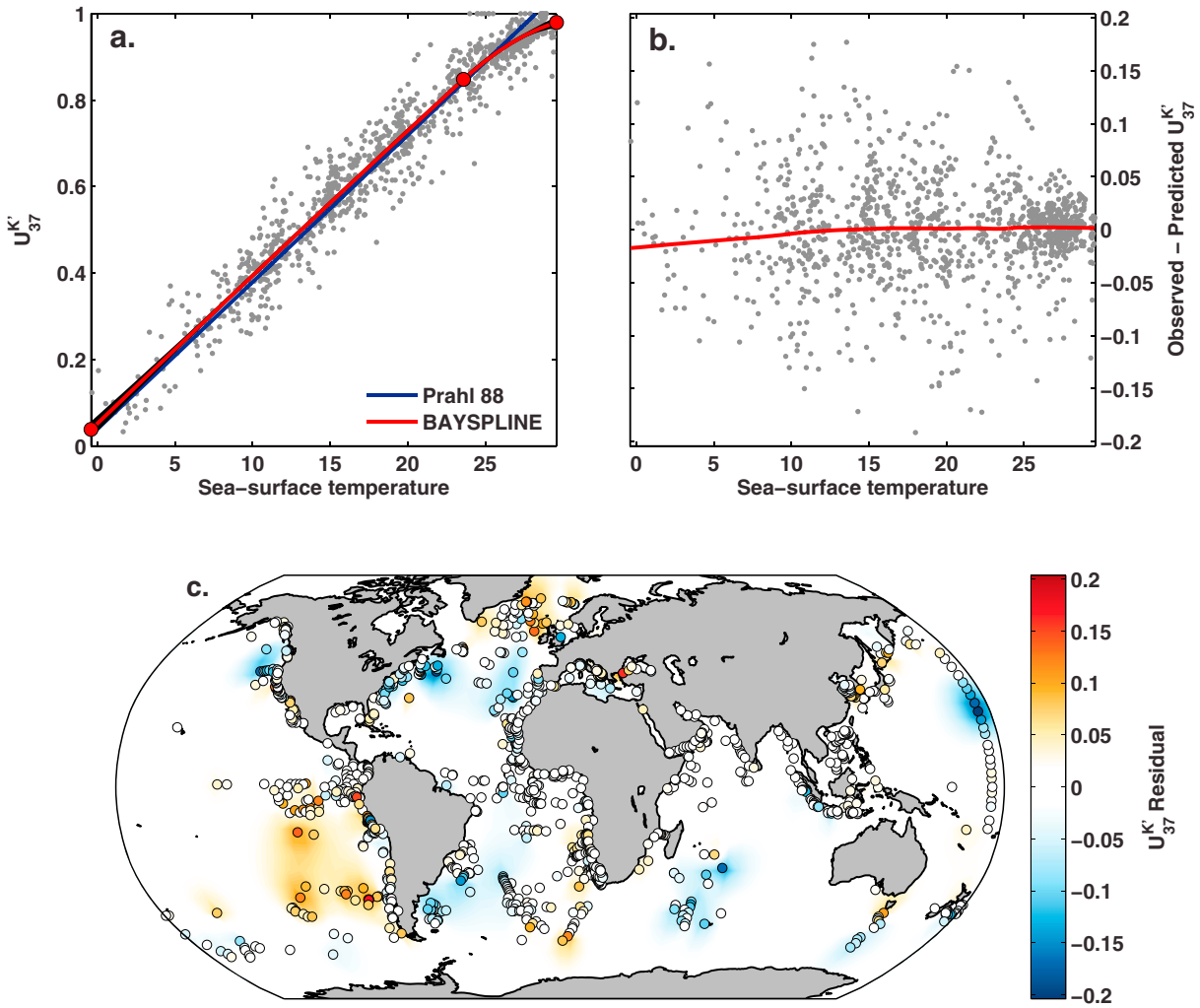

Figure 6. (a) The BAYSPLINE regression model, compared to the Prahl et al. (1988) calibration (dark blue line). Red line denotes the median spline, black lines beneath indicate the range of the spline fit ensemble. Red dots show the location of the knots. $U^{K'}_{37}$ core-top data, adjusted for seasonal bias, are plotted beneath the regression model in gray. (b) $U^{K'}_{37}$ residuals (observed $U^{K'}_{37}$-predicted $U^{K'}_{37}$) when applying BAYSPLINE. Red line represents a locally weighted scatterplot smoothing of the data with a span of 40% to highlight trends. There are no significant correlations between the residuals and sea surface temperature. (c) Global distribution of $U^{K'}_{37}$ residuals when applying BAYSPLINE, plotted as in Figure 3. As BAYSPLINE is nonlinear, residuals are plotted in $U^{K'}_{37}$ units; however, a $U^{K'}_{37}$ error of 0.2 is roughly 6° such that the color map is comparable with that of Figure 3.

Table 1
The Temperature Range, Slope, Number of Data Points (N) and Error of Previous $U^{K'}_{37}$ Calibrations and BAYSPLINE

Calibration	Range	Slope	*N*	1σ error
Prahl et al. (1988)	8–25°C	0.034	5	0.6°C
Müller et al. (1998)	0–29°C	0.033	370	1.5°C
Sonzogni et al. (1997)	24–29°C	0.023	40	0.7°C
Conte et al. (2006)	−1–29°C	0.034	592	1.1°C
BAYSPLINE	−0.4–29.6°C	0.034 below 23.4°C, decreasing to 0.011 at 29.6°C	1,344	1.4°C below 23.4°C, increasing to 4.4°C at 29.4°C

Note. Conte et al. (2006) refer to the core-top calibration in that study.

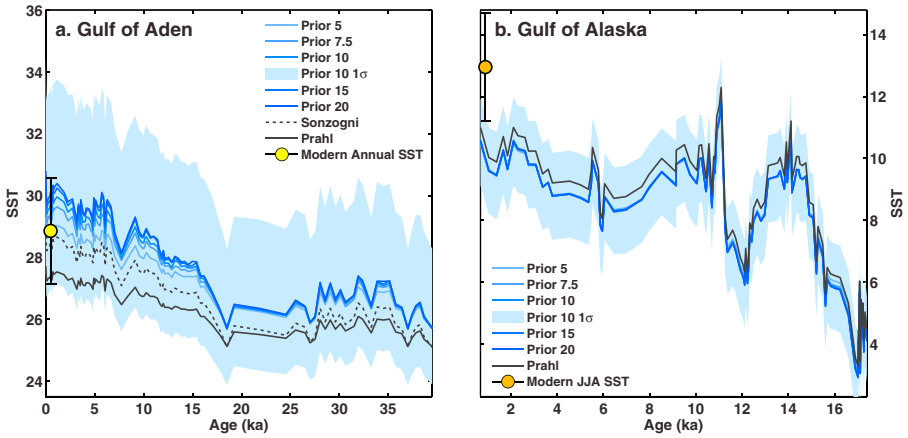

Figure 7. Example applications of BAYSPLINE to $U^{K'}_{37}$ data from (a) the Gulf of Aden (Tierney et al., 2016) and (b) the Gulf of Alaska (Praetorius et al., 2015). Blue lines represent results given different prior standard deviations. Light blue error bars represent 1σ uncertainties for a prior standard deviation of 10°C. Solid black line shows sea surface temperatures (SSTs) inferred from the Prahl et al. (1988) calibration, and dotted black line shows SSTs inferred from the Sonzogni et al. (1997) calibration (Gulf of Aden only). Yellow dot and orange dot with error bars represent the median and 1σ range of modern mean annual and July–August SSTs, respectively, at each core location.

One of the advantages of BAYSPLINE is that the calibration error is propagated into the calculation of SSTs and changes dynamically depending on the slope of the spline curve. In the Gulf of Aden example, the 1σ error on the warm Late Holocene estimates is 3.2°C, whereas the error during the cooler LGM is 2.4°C. These errors are larger than those associated with previous calibrations, but realistic considering that they account for slope attenuation, uncertainties in regression parameter estimation, and the variance in global core-top data. When we apply BAYSPLINE to data from the Gulf of Alaska (Praetorius et al., 2015), the 1σ error drops accordingly (to 1.4°C) as the slope increases to 0.034 (Figure 7b). In addition, there is virtually no sensitivity to the prior standard deviation choice at the low- to middle-range values of $U^{K'}_{37}$ found at this site, unless it is set to a quantity far lower than the standard deviation of the time series (e.g., 2°C; not shown). The low error and insensitivity to the prior indicate a dominance of the regression model likelihood whenever $U^{K'}_{37}$ is below a value of ~0.86 (roughly equivalent to 24°C). The Gulf of Alaska sits within the zone of the North Pacific in which $U^{K'}_{37}$ preferentially records summer temperatures (Figure 4) and BAYSPLINE is set to explicitly predict June–August SSTs. Modern summer SSTs are slightly higher than the median predictions by BAYSPLINE as well as Prahl et al. (1988), but they overlap with BAYSPLINE within uncertainty (Figure 7b). BAYSPLINE inference of June–August SSTs for the Gulf of Alaska site is consistent with the original interpretation of the authors, in which they note that core tops from the region clearly show a summer temperature bias (Praetorius et al., 2015).

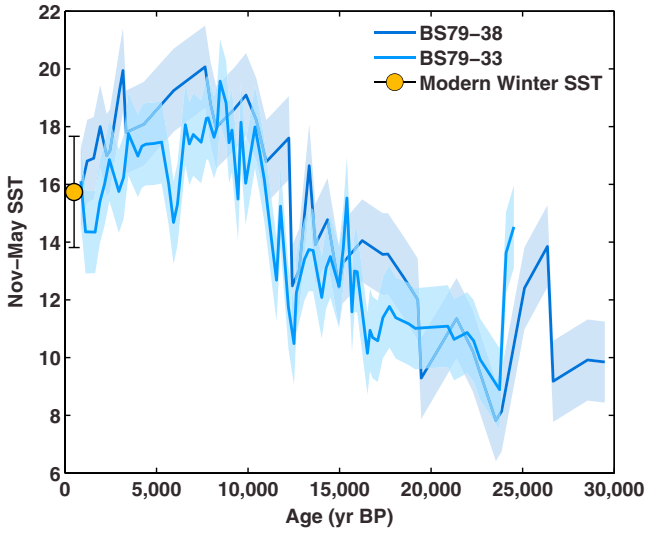

Figure 8. BAYSPLINE-$U^{K'}_{37}$ winter sea surface temperatures (SSTs) (with 1σ error bars) from two cores from the Tyrrhenian Sea (Mediterranean) (Cacho et al., 2001). Orange dot with error bar represents the median and 1σ range of modern November–May SSTs at the location of these cores. BP = before present.

Overall, these Late Quaternary examples demonstrate that BAYSPLINE produces reasonable results. Given $U^{K'}_{37}$ values below ~0.86, there is little sensitivity to the prior as the likelihood of the regression model dominates, and predictions are more or less comparable to those of previous linear calibrations. For $U^{K'}_{37}$ values above 0.86, the decreasing sensitivity to SST modeled by BAYSPLINE results in larger uncertainties and a greater reliance on the prior. However, it is important to note that even at the most extreme $U^{K'}_{37}$ values (~0.99) median SSTs vary by no more than 1–1.5°C. Thus, inference of SSTs from very high values of $U^{K'}_{37}$ is possible, albeit with large uncertainties. For example, the maximal $U^{K'}_{37}$ value of 1 predicts SSTs ranging from 27 to 39°C (90% confidence interval) with a prior standard deviation of 10°. This inference includes temperatures that may exceed the thermal tolerance for haptophyte algae, although the capacity for growth at high temperatures varies widely between studied strains (Conte et al., 1998), and we cannot know the maximum temperature

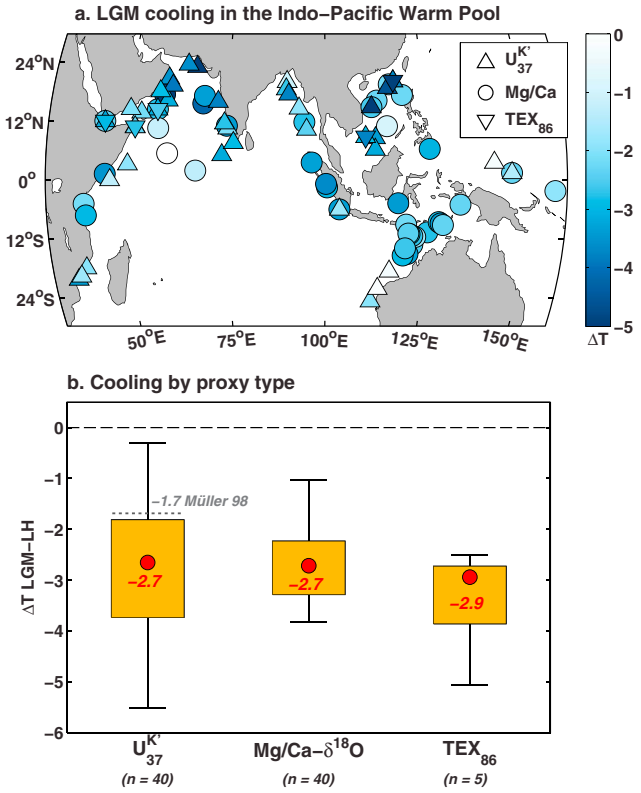

Figure 9. Multiproxy comparison of the magnitude of sea surface temperature change during the Last Glacial Maximum (LGM) (difference between 23–19 ka and 4–0 ka) in the Indo-Pacific Warm Pool region. $U^{K'}_{37}$ is calibrated with BAYSPLINE, Mg/Ca-δ^{18}O is calibrated with a multivariate regression (see the supporting information), and TEX_{86} is calibrated with the Tierney and Tingley (2015) sea surface temperature calibration. (a) Location and magnitude of cooling of individual proxy records. (b) Box plot of cooling by proxy type. Red dots and text denote median values. Boxes enclose 75% of the data, and whiskers denote the 90% confidence interval. Gray dotted line above the $U^{K'}_{37}$ box shows the median cooling using the Müller et al. (1998) calibration. The number of sites in each box is listed below the proxy labels.

tolerance of extinct coccolithophorids. Brassell (2014) noted that triunsaturated alkenones are present, albeit in very low abundance, at low-latitude sites during the middle Eocene, when independent indicators such as TEX_{86} indicate tropical SSTs of ~33° (Pearson et al., 2007), but are absent in the early Eocene when temperatures were presumably warmer. This may justify the use of a smaller prior standard deviation for very high values of $U^{K'}_{37}$, although, as noted in the Gulf of Aden example above, this can artificially restrict the range of the predicted values.

5. Implications for Paleoclimatic Interpretations

Three features distinguish BAYSPLINE from previous $U^{K'}_{37}$ calibrations: (1) explicit calibration of North Pacific, North Atlantic, and Mediterranean data to seasonal temperatures; (2) modeling of slope attenuation at high SSTs; and (3) propagation of errors in the regression model parameters and error variance, which allows for robust statistical assessment of inferred SSTs. All three of these features have an impact on paleoclimate interpretations derived from $U^{K'}_{37}$ data.

Inference of seasonal temperatures in the target regions identified here is largely consistent with the intuition of researchers pursuing $U^{K'}_{37}$-based climate reconstruction in these areas (e.g., Emeis et al., 2000; Haug et al., 2005; Praetorius et al., 2015). Calibration to a seasonal average thus simplifies interpretation and clarifies the appropriate season for comparison with climate model output. For example, Rosell-Melé et al. (2004) noted that $U^{K'}_{37}$ data from the Mediterranean region show a very large cooling during the LGM (−7 to −10°C), compared to other data at similar latitudes. Interpreted as a mean annual signal, the magnitude of this cooling is excessive when compared to model simulations (Rosell-Melé et al., 2004). Interpreted as a winter signal, the magnitude is reasonable, considering that pollen data from southern Europe show that LGM cooling was more pronounced in winter (Peyron et al., 1998). Application of BAYSPLINE to $U^{K'}_{37}$ data from the Tyrrhenian Sea (Cacho et al., 2001) demonstrates that Holocene values are in good agreement with modern winter SSTs, supporting a seasonal interpretation for these data, and indicate a wintertime LGM cooling of ~ −6 to −7°C (Figure 8).

BAYSPLINE's treatment of the slope attenuation is critical for the interpretation of $U^{K'}_{37}$ data from tropical locations, where traditional linear calibrations will underestimate the magnitude of SST change. To illustrate this, we investigate the magnitude of cooling during the LGM in the Indo-Pacific Warm Pool (IPWP), using multiple SST proxies from 77 sites (data from Bard et al., 1997; Budziak, 2001; Dahl & Oppo, 2006; de Garidel-Thoron et al., 2007; Gebregiorgis et al., 2016; Gibbons et al., 2014; Huguet et al., 2006; Kudrass et al., 2001; Mohtadi et al., 2010, 2014; Palmer & Pearson, 2003; Pelejero et al., 1999; Rippert et al., 2015; Romahn et al., 2014; Saraswat et al., 2013; Schulte & Müller, 2001; Shintani et al., 2008, 2011; Sonzogni et al., 1998; Stott et al., 2007; Tierney et al., 2016; Waelbroeck et al., 2009; Xu et al., 2008, 2010; Yamamoto et al., 2013). See the supporting information for details concerning the data compilation, which uses methodology from Bemis et al. (1998), Bronk Ramsey (1995, 2008), Tierney et al. (2016), Holloway et al. (2016), Khider et al. (2015), Regenberg et al. (2014), Reimer et al. (2013), Tierney and Tingley (2015). Application of the Müller et al. (1998) calibration to the $U^{K'}_{37}$ data from the IPWP suggests an average LGM cooling of only −1.6°C (Figure 9). This value is much smaller than estimates based on paired Mg/Ca-δ^{18}O measurements of planktic foraminifera (−2.7°C using the calibration of Tierney et al., 2016; see the supporting information for details) and TEX_{86} (−2.9°C using the latest BAYSPAR SST calibration, Tierney & Tingley, 2015) from the same region and in some cases, from the same locations (Figure 9). Applying BAYSPLINE to the $U^{K'}_{37}$ data reconciles this apparent difference, bringing the median estimate to −2.7°C (Figure 9b). BAYSPLINE also facilitates a probabilistic approach to categorizing the magnitude of cooling in the IPWP; for example, we can state, based on the $U^{K'}_{37}$ data, that there is a 94% probability that mean IPWP cooling exceeded −2°, but only a 10% probability that it exceeded −4°.

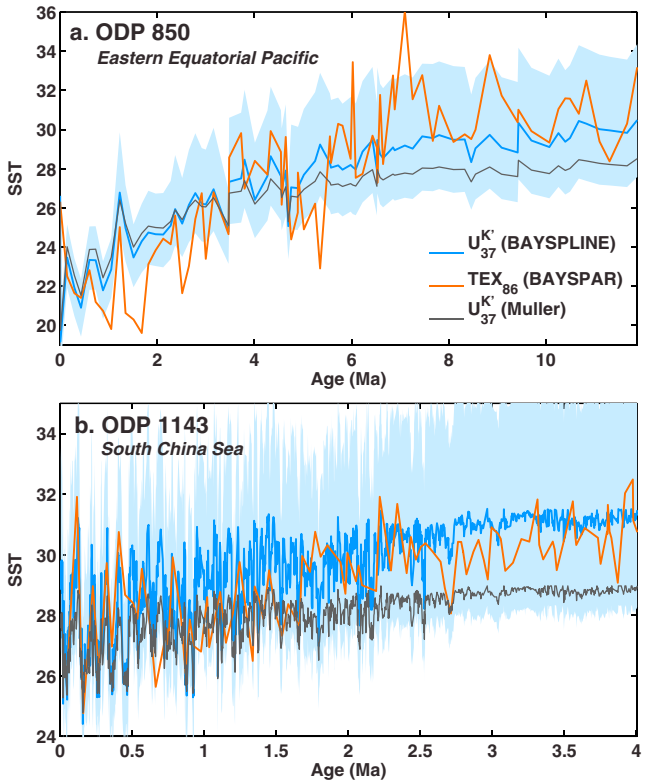

Figure 10. Miocene and Pliocene $U^{K'}_{37}$ and TEX_{86} data from (a) the eastern equatorial Pacific (Ocean Drilling Program (ODP) 850, Zhang et al., 2014) and (b) the South China Sea (ODP 1143, Li et al., 2011; O'Brien et al., 2014; Zhang et al., 2014). Blue line shows median inferred SSTs from BAYSPLINE, light blue error bars represent 1σ uncertainties for a prior standard deviation of 10°C, orange line shows median inferred SSTs from BAYSPAR (Tierney & Tingley, 2015), and dark gray line shows inferred sea surface temperatures from the Müller et al. (1998) calibration.

In this IPWP compilation, $U^{K'}_{37}$ and Mg/Ca-δ^{18}O are represented equally, making the comparison between these two proxy systems especially apt. BAYSPLINE $U^{K'}_{37}$ estimates show greater variance than those derived from Mg/Ca-δ^{18}O (Figure 9b), both because the $U^{K'}_{37}$ sites span a greater range of apparent temperatures, and the uncertainties in the BAYSPLINE calibration are larger at the warm end. On the other hand, the Mg/Ca-δ^{18}O regression does not fully propagate uncertainties, so the confidence intervals are likely too small. The LGM TEX_{86} estimate is also more constrained than that of $U^{K'}_{37}$ (Figure 9b), but this is because there are only five TEX_{86} sites available (Figure 9a and see Table S1).

This LGM exercise demonstrates that BAYSPLINE produces similar temperature estimates in the tropics as other geochemical proxies. In contrast, the Müller et al. (1998) calibration predicts a cooling that does not overlap with the TEX_{86} estimates at all and has a low probability (10%) of being consistent with the Mg/Ca-δ^{18}O estimates (Figure 9b). This highlights the fact that the most widely used $U^{K'}_{37}$ calibrations (Müller et al., 1998; Prahl et al., 1988) underestimate tropical temperature anomalies by about 40%. As $U^{K'}_{37}$ data form a large portion of the available tropical SST proxy data spanning the LGM, or more broadly speaking, the Late Quaternary, BAYSPLINE will impact multiproxy syntheses (e.g., Shakun & Carlson, 2010; Waelbroeck et al., 2009) and analyses derived from such products, such as estimates of Earth climate sensitivity (Hargreaves et al., 2012; Schmittner et al., 2011).

BAYSPLINE also modifies interpretations of SSTs during past warm climate regimes. For example, there is an ongoing debate regarding the magnitude of warming across the tropical Pacific during the late Miocene and Pliocene that has largely fallen on proxy lines (Brierley et al., 2015; O'Brien et al., 2014; Ravelo et al., 2014; Zhang et al., 2014). In particular, the TEX_{86} paleothermometer records larger-magnitude changes than both $U^{K'}_{37}$ and Mg/Ca, leading to speculation that it is capturing deeper-water temperatures (Ravelo et al., 2014). However, the tropical Pacific sites in question contain high $U^{K'}_{37}$ values, such that linear calibrations likely underestimate variability. Applying BAYSPLINE to two of these key sites (Ocean Drilling Program (ODP) 850 in the eastern equatorial Pacific and ODP 1143 in the South China Sea) demonstrates that our new calibration produces substantially better agreement with the TEX_{86} estimates (Figure 10). At ODP 850, the magnitude of cooling between the Miocene (12–6 Ma) and the latest Pleistocene data (0.5–0 Ma) from BAYSPLINE (−6.7 ± 1.6°C, 1σ) agrees within uncertainty with the TEX_{86}-estimated change (−6.9 ± 0.9°C, 1σ), whereas the cooling estimated from Müller et al. (1998) is only −4.9°C (Figure 10a). At Site ODP 1143, application of BAYSPLINE produces dramatically different results as $U^{K'}_{37}$ values approach saturation during the Pliocene (4–2.6 Ma in Figure 10b). Here the magnitude of cooling between the Pliocene data (4–2.6 Ma) and the latest Pleistocene data (0–0.5 Ma) estimated by BAYSPLINE (−3.5 ± 0.8°C, 1σ) is actually larger than the TEX_{86} value (−2.4 ± 0.2, 1σ). In contrast, the Müller et al. (1998)-estimated cooling is only −1.9°C and yields SSTs that are 2° cooler than the TEX_{86} predictions in the Pliocene (Figure 10b). The magnitude of TEX_{86} and $U^{K'}_{37}$-inferred glacial-interglacial variability is also in better agreement when BAYSPLINE is used (Figure 10b). Overall, this example shows that perceived differences between $U^{K'}_{37}$ and TEX_{86} in the warm Miocene and Pliocene may be simply due to underestimation of $U^{K'}_{37}$-SST changes by linear calibrations, and conversely, TEX_{86} can act as a reasonable tracer for SSTs in the right setting. This said, there are still locations where TEX_{86} arguably records shallow thermocline variability and $U^{K'}_{37}$ and TEX_{86} patterns diverge substantially (dos Santos et al., 2010; Tierney et al., 2016).

6. Conclusions

Our reexamination of core-top $U^{K'}_{37}$ demonstrates that seasonal production and slope attenuation at high temperatures are fundamental features of the data that must be explicitly accounted for to avoid calibration bias. We do not detect slope attenuation at cold temperatures, but this could be due to undersampling of

the high-latitude oceans, in particular, the Southern Ocean. We propose as a solution a Bayesian calibration for $U_{37}^{K'}$ based on B-splines (BAYSPLINE) that accommodates these features. Through application to example time series, we show that BAYSPLINE produces reasonable estimates of SSTs and improves inference in the tropical oceans. In addition to its treatment of seasonality and slope attenuation, BAYSPLINE offers an advantage in that it produces ensemble-based results that capture the uncertainty in the core-top regression. These ensembles provide meaningful uncertainty bounds and can be used for statistical reasoning. Given that $U_{37}^{K'}$ measurements comprise a substantial portion of late Cenozoic paleotemperature data, application of BAYSPLINE will enhance and improve our ability to identify the fundamental mechanisms driving climatic change in the recent geologic past.

Appendix A: Bayesian Analysis

As stated in the main text, the BAYSPLINE model is based on a Bayesian regression with B-splines, such that

$$p(\boldsymbol{\beta}, \tau^2|\mathbf{Y}, \{B(\mathbf{X})\}) \propto p(\mathbf{Y}|\{B(\mathbf{X})\}, \boldsymbol{\beta}, \tau^2) \cdot p(\boldsymbol{\beta}, \tau^2). \tag{A1}$$

The likelihood is a Normal distribution:

$$p(\mathbf{Y}|\{B(\mathbf{X})\}, \boldsymbol{\beta}, \tau^2) \sim \mathcal{N}(\{B(\mathbf{X})\}\boldsymbol{\beta}, \sigma^2\mathrm{I}), \tag{A2}$$

and we use conjugate priors (Gelman et al., 2003) for $\boldsymbol{\beta}$ and τ^2, which are normal and inverse gamma, respectively:

$$\begin{aligned}\boldsymbol{\beta} &\sim \mathcal{N}(\mu_0, \sigma_0^2\mathrm{I})\\ \tau^2 &\sim \mathcal{IG}(a_0, b_0).\end{aligned} \tag{A3}$$

The prior means for the B-spline coefficients (μ_0) were derived from an ordinary least squares estimate. The prior standard deviation for the B-spline coefficients (σ_0^2) and for τ^2 (a_0, b_0) was set to large values to keep the priors relatively uninformative, such that the core-top data are largely responsible for informing the model (see Figure S1). Multiplying the prior and the likelihood and solving for the full conditional posteriors (Gelman et al., 2003) yields

$$\begin{aligned}&\boldsymbol{\beta}|\cdot \sim \mathcal{N}(\boldsymbol{\Psi}\mathbf{V}, \mathbf{V}),\\ &\boldsymbol{\Psi} = \mu_0\sigma_0^{-2}\mathrm{I} + \{B(\mathbf{X})\}^T\mathbf{Y}\tau^{-2}\\ &\mathbf{V} = \sigma_0^{-2}\mathrm{I} + \{B(\mathbf{X})\}^T\{B(\mathbf{X})\}\tau^{-2}.\\ &\tau^2|\cdot \sim \mathcal{IG}\left(a_0 + \frac{N}{2}, b_0 + \frac{1}{2}\cdot(\mathbf{Y} - \{B(\mathbf{X})\}\boldsymbol{\beta})^T(\mathbf{Y} - \{B(\mathbf{X})\}\boldsymbol{\beta})\right).\end{aligned} \tag{A4}$$

Inference of the posterior then proceeds by specifying an initial value for one of the unknown parameters and using a Gibbs sampler (Gelman et al., 2003) to sequentially draw from the full conditionals in turn. We ensured monotonicity in the spline via rejection sampling (Gelman et al., 2003). We ran five separate chains of 5,000 draws each, discarding the first 200 draws of each chain as burn-in. The $\hat{R}$ statistic (Gelman et al., 2003) indicated that convergence was achieved under these conditions ($\hat{R}$ =1.000 for all parameters), at which point the chains were concatenated and then thinned by a factor of 16 to remove serial correlation. The resulting posteriors for $\boldsymbol{\beta}$ and τ^2 consist of 1,500 draws. Figure S1 shows the prior and posterior distributions and demonstrates that the data effectively constrain each regression parameter.

For prediction of SSTs from $U_{37}^{K'}$, we invert the BAYSPLINE model using another application of Bayes' rule:

$$p(\mathbf{X}_{\mathrm{new}}|\mathbf{Y}_{\mathrm{new}}) \propto p(\mathbf{Y}_{\mathrm{new}}|\{B(\mathbf{X})\}, \boldsymbol{\beta}, \tau^2) \cdot p(\mathbf{X}_{\mathrm{new}}). \tag{A5}$$

Due to the B-spline transformation, posterior distribution does not have an analytic solution. Thus, we use the Metropolis algorithm (Gelman et al., 2003) to calculate the posterior. For each round of sampling, a proposal of SST values is drawn from a normal jumping distribution, and its posterior probability is evaluated against an initial SST starting distribution. The proposal is either accepted or rejected, and the chain continues until convergence is reached. The $U_{37}^{K'}$ observations are treated as independent; that is, the proposal evaluation process is separate for each data point in the time series. During Metropolis sampling, we extrapolate the spline function linearly beyond its lower and upper limits of −0.4°C and 29.6°C, respectively, to allow for prediction of temperatures outside the range of modern SST values. The Metropolis sampling mixes across uncertainties

in the posterior model parameters by running parallel chains of $N = 500$ to sample every third paired posterior draw of β and τ^2 (for a total M chains = 500). The first half of each chain ($N = 250$) is discarded as burn-in. The standard deviation of the jumping distribution (J_σ) was set to yield an acceptance rate between 40 and 50%, in line with the recommendations of Gelman et al. (2003). These settings result in adequate convergence ($\hat{R} = 1.008–1.08$) while minimizing computational time (about 25–40 s on an average desktop computer). Mixing results across all 1,500 posterior samples and increasing the length of the chains by an order of magnitude ($N = 5,000$), respectively, afforded no substantial improvement in convergence.

Acknowledgments
We thank Elizabeth Sikes and two anonymous reviewers for their comments and suggestions and Hope Ianiri and Paul Zander for assistance with the laboratory analyses and data compilation. This work was supported by National Science Foundation grants AGS 1602301 and AGS 1443176, the Heising-Simons Foundation, and the Packard Fellowship in Science and Engineering to J. T. BAYSPLINE code (in Matlab) is publicly available for download from the first author's GitHub site: http://github.com/jesstierney. A Python and GUI implementation are under development. The global alkenone core-top data set is available as a Data Set S1 in the supporting information, as well as online in the NOAA NCEI Paleoclimatology archive: https://www.ncdc.noaa.gov/paleo/study/23370.

References

Annan, J., & Hargreaves, J. (2013). A new global reconstruction of temperature changes at the Last Glacial Maximum. *Climate of the Past*, *9*(1), 367–376.

Arz, H. W., Lamy, F., Pätzold, J., Müller, P. J., & Prins, M. (2003). Mediterranean moisture source for an early-Holocene humid period in the northern Red Sea. *Science*, *300*(5616), 118–121.

Banzon, V., Smith, T. M., Chin, T. M., Liu, C., & Hankins, W. (2016). A long-term record of blended satellite and in situ sea-surface temperature for climate monitoring, modeling and environmental studies. *Earth System Science Data*, *8*(1), 165–176.

Bard, E. (2001). Comparison of alkenone estimates with other paleotemperature proxies. *Geochemistry, Geophysics Geosystems*, *2*(1), 1002.

Bard, E., Rostek, F., & Sonzogni, C. (1997). Interhemispheric synchrony of the last deglaciation inferred from alkenone palaeothermometry. *Nature*, *385*(6618), 707–710.

Bard, E., Rostek, F., Turon, J.-L., & Gendreau, S. (2000). Hydrological impact of Heinrich events in the subtropical northeast Atlantic. *Science*, *289*(5483), 1321–1324.

Barron, J. A., Heusser, L., Herbert, T., & Lyle, M. (2003). High-resolution climatic evolution of coastal northern California during the past 16,000 years. *Paleoceanography*, *18*(1), 1020. https://doi.org/10.1029/2002PA000768

Barrows, T. T., Lehman, S. J., Fifield, L. K., & De Deckker, P. (2007). Absence of cooling in New Zealand and the adjacent ocean during the Younger Dryas chronozone. *Science*, *318*(5847), 86–89.

Becker, K. W., Lipp, J. S., Versteegh, G. J., Wörmer, L., & Hinrichs, K.-U. (2015). Rapid and simultaneous analysis of three molecular sea surface temperature proxies and application to sediments from the Sea of Marmara. *Organic Geochemistry*, *85*, 42–53.

Bemis, B. E., Spero, H. J., Bijma, J., & Lea, D. W. (1998). Reevaluation of the oxygen isotopic composition of planktonic foraminifera: Experimental results and revised paleotemperature equations. *Paleoceanography*, *13*(2), 150–160.

Bendle, J., & Rosell-Melé, A. (2004). Distributions of U^{K}_{37} and $U^{K'}_{37}$ in the surface waters and sediments of the Nordic Seas: Implications for paleoceanography. *Geochemistry, Geophysics Geosystems*, *5*, Q11013. https://doi.org/10.1029/2004GC00074

Bendle, J. A., & Rosell-Melé, A. (2007). High-resolution alkenone sea surface temperature variability on the North Icelandic Shelf: Implications for Nordic Seas palaeoclimatic development during the Holocene. *The Holocene*, *17*(1), 9–24.

Benthien, A., & Müller, P. J. (2000). Anomalously low alkenone temperatures caused by lateral particle and sediment transport in the Malvinas Current region, western Argentine Basin. *Deep Sea Research Part I: Oceanographic Research Papers*, *47*(12), 2369–2393.

Brassell, S. C., Eglinton, G., Marlowe, I. T., Pflaumann, U., & Sarnthein, M. (1986). Molecular stratigraphy—A new tool for climatic assessment. *Nature*, *320*(6058), 129–133.

Brassell, S. (2014). Climatic influences on the Paleogene evolution of alkenones. *Paleoceanography*, *29*, 255–272. https://doi.org/10.1002/2013PA002576

Brierley, C., Burls, N., Ravelo, C., & Fedorov, A. (2015). Pliocene warmth and gradients. *Nature Geoscience*, *8*(6), 419–420.

Bronk Ramsey, C. (1995). Radiocarbon calibration and analysis of stratigraphy: The OxCal program. *Radiocarbon*, *37*(2), 425–430.

Bronk Ramsey, C. (2008). Deposition models for chronological records. *Quaternary Science Reviews*, *27*(1), 42–60.

Budziak, D. (2001). Late Quaternary monsoonal climate and related variations in paleoproductivity and alkenone-derived sea-surface temperatures in the western Arabian Sea (Ph.D. thesis), University of Bremen.

Budziak, D., Schneider, R. R., Rostek, F., Müller, P. J., Bard, E., & Wefer, G. (2000). Late Quaternary insolation forcing on total organic carbon and C_{37} alkenone variations in the Arabian Sea. *Paleoceanography*, *15*(3), 307–321.

Cacho, I., Pelejero, C., Grimalt, J. O., Calafat, A., & Canals, M. (1999). C_{37} alkenone measurements of sea surface temperature in the Gulf of Lions (NW Mediterranean). *Organic Geochemistry*, *30*(7), 557–566.

Cacho, I., Grimalt, J. O., Pelejero, C., Canals, M., Sierro, F. J., Flores, J. A., & Shackleton, N. (1999). Dansgaard-Oeschger and Heinrich event imprints in Alboran Sea paleotemperatures. *Paleoceanography*, *14*(6), 698–705.

Cacho, I., Grimalt, J. O., Canals, M., Sbaffi, L., Shackleton, N. J., Schönfeld, J., & Zahn, R. (2001). Variability of the western Mediterranean Sea surface temperature during the last 25,000 years and its connection with the Northern Hemisphere climatic changes. *Paleoceanography*, *16*(1), 40–52.

Calvo, E., Pelejero, C., Herguera, J. C., Palanques, A., & Grimalt, J. O. (2001). Insolation dependence of the southeastern Subtropical Pacific sea surface temperature over the last 400 kyrs. *Geophysical Research Letters*, *28*(12), 2481–2484.

Calvo, E., Pelejero, C., De Deckker, P., & Logan, G. A. (2007). Antarctic deglacial pattern in a 30 kyr record of sea surface temperature offshore South Australia. *Geophysical Research Letters*, *34*, L13707. https://doi.org/10.1029/2007GL029937

Caniupán, M., Lamy, F., Lange, C., Kaiser, J., Arz, H., Kilian, R., et al. (2011). Millennial-scale sea surface temperature and Patagonian Ice Sheet changes off southernmost Chile (53°S) over the past ~60 kyr. *Paleoceanography*, *26*, PA3221. https://doi.org/10.1029/2010PA002049

Chapman, M., Shackleton, N., Zhao, M., & Eglinton, G. (1996). Faunal and alkenone reconstructions of subtropical North Atlantic surface hydrography and paleotemperature over the last 28 kyr. *Paleoceanography*, *11*(3), 343–357.

Chen, W., Mohtadi, M., Schefuß, E., & Mollenhauer, G. (2014). Organic-geochemical proxies of sea surface temperature in surface sediments of the tropical eastern Indian Ocean. *Deep Sea Research Part I: Oceanographic Research Papers*, *88*, 17–29.

Conte, M. H., Thompson, A., Lesley, D., & Harris, R. P. (1998). Genetic and physiological influences on the alkenone/alkenoate versus growth temperature relationship in Emiliania huxleyi and Gephyrocapsa oceanica. *Geochimica et Cosmochimica Acta*, *62*(1), 51–68.

Conte, M. H., Sicre, M.-A., Rühlemann, C., Weber, J. C., Schulte, S., Schulz-Bull, D., & Blanz, T. (2006). Global temperature calibration of the alkenone unsaturation index ($U^{K'}_{37}$) in surface waters and comparison with surface sediments. *Geochemistry, Geophysics, Geosystems*, *7*, Q02005. https://doi.org/10.1029/2005GC001054

Dahl, K. A., & Oppo, D. W. (2006). Sea surface temperature pattern reconstructions in the Arabian Sea. *Paleoceanography*, *21*, PA1014. https://doi.org/10.1029/2005PA001162

de Garidel-Thoron, T., Rosenthal, Y., Beaufort, L., Bard, E., Sonzogni, C., & Mix, A. C. (2007). A multiproxy assessment of the western equatorial Pacific hydrography during the last 30 kyr. *Paleoceanography*, *22*, PA3204. https://doi.org/10.1029/2006PA001269

Dekens, P. S., Lea, D. W., Pak, D. K., & Spero, H. J. (2002). Core top calibration of Mg/Ca in tropical foraminifera: Refining paleotemperature estimation. *Geochemistry, Geophysics, Geosystems*, *3*(4), 1–29. https://doi.org/10.1029/2001GC000200

Doose, H., Prahl, F. G., & Lyle, M. W. (1997). Biomarker temperature estimates for modern and last glacial surface waters of the California Current system between 33 and 42°N. *Paleoceanography*, *12*(4), 615–622.

dos Santos, R. A. L., Prange, M., Castañeda, I. S., Schefuß, E., Mulitza, S., Schulz, M., et al. (2010). Glacial–interglacial variability in Atlantic meridional overturning circulation and thermocline adjustments in the tropical North Atlantic. *Earth and Planetary Science Letters*, *300*(3), 407–414.

Dubois, N., Kienast, M., Normandeau, C., & Herbert, T. D. (2009). Eastern equatorial Pacific cold tongue during the Last Glacial Maximum as seen from alkenone paleothermometry. *Paleoceanography*, *24*, PA4207. https://doi.org/10.1029/2009PA001781

Emeis, K.-C., Struck, U., Schulz, H.-M., Rosenberg, R., Bernasconi, S., Erlenkeuser, H., et al. (2000). Temperature and salinity variations of Mediterranean Sea surface waters over the last 16,000 years from records of planktonic stable oxygen isotopes and alkenone unsaturation ratios, Palaeogeography. *Palaeoclimatology Palaeoecology*, *158*(3), 259–280.

Emeis, K.-C., Struck, U., Blanz, T., Kohly, A., & Voß, M. (2003). Salinity changes in the central Baltic Sea (NW Europe) over the last 10000 years. *The Holocene*, *13*(3), 411–421.

Epstein, B., d'Hondt, S., & Hargraves, P. (2001). The possible metabolic role of C_{37} alkenones in Emiliania huxleyi. *Organic Geochemistry*, *32*(6), 867–875.

Fallet, U., Castañeda, I. S., Henry-Edwards, A., Richter, T. O., Boer, W., Schouten, S., & Brummer, G.-J. (2012). Sedimentation and burial of organic and inorganic temperature proxies in the Mozambique Channel, SW Indian Ocean. *Deep Sea Research Part I: Oceanographic Research Papers*, *59*, 37–53.

Filippova, A., Kienast, M., Frank, M., & Schneider, R. (2016). Alkenone paleothermometry in the North Atlantic: A review and synthesis of surface sediment data and calibrations. *Geochemistry, Geophysics, Geosystems*, *17*, 1370–1382. https://doi.org/10.1002/2015GC006106

Fraser, N., Kuhnt, W., Holbourn, A., Bolliet, T., Andersen, N., Blanz, T., & Beaufort, L. (2014). Precipitation variability within the West Pacific Warm Pool over the past 120 ka: Evidence from the Davao Gulf, southern Philippines. *Paleoceanography*, *29*, 1094–1110. https://doi.org/10.1002/2013PA002599

Gebregiorgis, D., Hathorne, E. C., Sijinkumar, A., Nath, B. N., Nürnberg, D., & Frank, M. (2016). South Asian summer monsoon variability during the last ~54 kyrs inferred from surface water salinity and river runoff proxies. *Quaternary Science Reviews*, *138*, 6–15.

Gelman, A., Carlin, J., Stern, H., & Rubin, D. (2003). *Bayesian data analysis* (2nd ed.). Boca Raton: Chapman & Hall/CRC.

Gibbons, F. T., Oppo, D. W., Mohtadi, M., Rosenthal, Y., Cheng, J., Liu, Z., & Linsley, B. K. (2014). Deglacial $\delta^{18}O$ and hydrologic variability in the tropical Pacific and Indian Oceans. *Earth and Planetary Science Letters*, *387*, 240–251.

Goñi, M. A., Hartz, D. M., Thunell, R. C., & Tappa, E. (2001). Oceanographic considerations for the application of the alkenone-based paleotemperature $U^{K'}_{37}$ index in the Gulf of California. *Geochimica et Cosmochimica Acta*, *65*(4), 545–557.

Gutiérrez, D., Bouloubassi, I., Sifeddine, A., Purca, S., Goubanova, K., Graco, M., et al. (2011). Coastal cooling and increased productivity in the main upwelling zone off Peru since the mid-twentieth century. *Geophysical Research Letters*, *38*, L07603. https://doi.org/10.1029/2010GL046324

Harada, N., Ahagon, N., Sakamoto, T., Uchida, M., Ikehara, M., & Shibata, Y. (2006). Rapid fluctuation of alkenone temperature in the southwestern Okhotsk Sea during the past 120 ky. *Global and Planetary Change*, *53*(1), 29–46.

Hargreaves, J. C., Annan, J. D., Yoshimori, M., & Abe-Ouchi, A. (2012). Can the Last Glacial Maximum constrain climate sensitivity? *Geophysical Research Letters*, *39*, L24702. https://doi.org/10.1029/2012GL053872

Haug, G. H., Ganopolski, A., Sigman, D. M., Rosell-Mele, A., Swann, G. E., Tiedemann, R., et al. (2005). North Pacific seasonality and the glaciation of North America 2.7 million years ago. *Nature*, *433*(7028), 821–825.

Herbert, T. (2001). Review of alkenone calibrations (culture, water column, and sediments). *Geochemistry, Geophysics, Geosystems*, *2*, 1055. https://doi.org/10.1029/2000GC000055

Herbert, T., Schuffert, J., Thomas, D., Lange, C., Weinheimer, A., Peleo-Alampay, A., & Herguera, J.-C. (1998). Depth and seasonality of alkenone production along the California margin inferred from a core top transect. *Paleoceanography*, *13*(3), 263–271.

Herbert, T., Schuffert, J., Andreasen, D., Heusser, L., Lyle, M., Mix, A., et al. (2001). Collapse of the California Current during glacial maxima linked to climate change on land. *Science*, *293*(5527), 71–76.

Herbert, T. D. (2003). Alkenone paleotemperature determinations. *Treatise on Geochemistry*, *6*, 391–432.

Ho, S. L., Mollenhauer, G., Lamy, F., Martínez-Garcia, A., Mohtadi, M., Gersonde, R., et al. (2012). Sea surface temperature variability in the Pacific sector of the Southern Ocean over the past 700 kyr. *Paleoceanography*, *27*, PA4202. https://doi.org/10.1029/2012PA002317

Ho, S. L., Mollenhauer, G., Fietz, S., Martínez-Garcia, A., Lamy, F., Rueda, G., et al. (2014). Appraisal of TEX_{86} and TEX^{L}_{86} thermometries in subpolar and polar regions. *Geochimica et Cosmochimica Acta*, *131*, 213–226.

Hoefs, M. J., Versteegh, G. J., Rijpstra, W. I. C., Leeuw, J. W., & Damsté, J. S. S. (1998). Postdepositional oxic degradation of alkenones: Implications for the measurement of palaeo sea surface temperatures. *Paleoceanography*, *13*(1), 42–49.

Holloway, M. D., Sime, L. C., Singarayer, J. S., Tindall, J. C., & Valdes, P. J. (2016). Reconstructing paleosalinity from $\delta^{18}O$: Coupled model simulations of the Last Glacial Maximum, Last Interglacial and Late Holocene. *Quaternary Science Reviews*, *131*, 350–364.

Horikawa, K., Minagawa, M., Murayama, M., Kato, Y., & Asahi, H. (2006). Spatial and temporal sea-surface temperatures in the eastern equatorial Pacific over the past 150 kyr. *Geophysical research letters*, *33*, L13605. https://doi.org/10.1029/2006GL025948

Huang, C.-Y., Wu, S.-F., Zhao, M., Chen, M.-T., Wang, C.-H., Tu, X., & Yuan, P. B. (1997). Surface ocean and monsoon climate variability in the South China Sea since the last glaciation. *Marine Micropaleontology*, *32*(1), 71–94.

Huguet, C., Kim, J.-H., Sinninghe Damsté, J. S., & Schouten, S. (2006). Reconstruction of sea surface temperature variations in the Arabian Sea over the last 23 kyr using organic proxies (TEX_{86} and $U^{K'}_{37}$). *Paleoceanography*, *21*, PA3003. https://doi.org/10.1029/2005PA001215

Ikehara, M., Kawamura, K., Ohkouchi, N., Kimoto, K., Murayama, M., Nakamura, T., et al. (1997). Alkenone sea surface temperature in the Southern Ocean for the last two deglaciations. *Geophysical Research Letters*, *24*(6), 679–682.

Jaeschke, A., Rühlemann, C., Arz, H., Heil, G., & Lohmann, G. (2007). Coupling of millennial-scale changes in sea surface temperature and precipitation off northeastern Brazil with high-latitude climate shifts during the last glacial period. *Paleoceanography*, *22*, PA4206. https://doi.org/10.1029/2006PA001391

Jaeschke, A., Wengler, M., Hefter, J., Ronge, T. A., Geibert, W., Mollenhauer, G., et al. (2017). A biomarker perspective on dust, productivity, and sea surface temperature in the Pacific sector of the Southern Ocean. *Geochimica et Cosmochimica Acta*, *204*, 120–139.

Kaiser, J., Lamy, F., & Hebbeln, D. (2005). A 70-kyr sea surface temperature record off southern Chile (Ocean Drilling Program Site 1233). *Paleoceanography*, *20*, PA4009. https://doi.org/10.1029/2005PA001146

Kaiser, J., Schefuß, E., Lamy, F., Mohtadi, M., & Hebbeln, D. (2008). Glacial to Holocene changes in sea surface temperature and coastal vegetation in north central Chile: High versus low latitude forcing. *Quaternary Science Reviews*, *27*(21), 2064–2075.

Kaiser, J., Ruggieri, N., Hefter, J., Siegel, H., Mollenhauer, G., Arz, H. W., & Lamy, F. (2014). Lipid biomarkers in surface sediments from the Gulf of Genoa, Ligurian sea (NW Mediterranean sea) and their potential for the reconstruction of palaeo-environments. *Deep Sea Research Part I: Oceanographic Research Papers*, *89*, 68–83.

Kennedy, J. A., & Brassell, S. C. (1992). Molecular records of twentieth-century El Niño events in laminated sediments from the Santa Barbara basin. *Nature*, *357*(6373), 62.

Khider, D., Huerta, G., Jackson, C., Stott, L., & Emile-Geay, J. (2015). A Bayesian, multivariate calibration for Globigerinoides ruber Mg/Ca. *Geochemistry, Geophysics, Geosystems*, *16*, 2916–2932. https://doi.org/10.1002/2015GC005844

Kienast, M., Kienast, S. S., Calvert, S. E., Eglinton, T. I., Mollenhauer, G., Francois, R., & Mix, A. C. (2006). Eastern Pacific cooling and Atlantic overturning circulation during the last deglaciation. *Nature*, *443*(7113), 846–849.

Kienast, M., MacIntyre, G., Dubois, N., Higginson, S., Normandeau, C., Chazen, C., & Herbert, T. (2012). Alkenone unsaturation in surface sediments from the eastern equatorial Pacific: Implications for SST reconstructions. *Paleoceanography*, *27*, PA1210. https://doi.org/10.1029/2011PA002254

Kienast, S. S., & McKay, J. L. (2001). Sea surface temperatures in the subarctic northeast Pacific reflect millennial-scale climate oscillations during the last 16 kyrs. *Geophysical Research Letters*, *28*(8), 1563–1566.

Kim, J., Van der Meer, J., Schouten, S., Helmke, P., Willmott, V., Sangiorgi, F., et al. (2010). New indices and calibrations derived from the distribution of crenarchaeal isoprenoid tetraether lipids: Implications for past sea surface temperature reconstructions. *Geochimica et Cosmochimica Acta*, *74*(16), 4639–4654.

Kim, J.-H., Schneider, R. R., Hebbeln, D., Müller, P. J., & Wefer, G. (2002). Last deglacial sea-surface temperature evolution in the Southeast Pacific compared to climate changes on the South American continent. *Quaternary Science Reviews*, *21*(18), 2085–2097.

Kim, J.-H., Schneider, R. R., Müller, P. J., & Wefer, G. (2002). Interhemispheric comparison of deglacial sea-surface temperature patterns in Atlantic eastern boundary currents. *Earth and Planetary Science Letters*, *194*(3), 383–393.

Kim, J.-H., Schneider, R. R., Mulitza, S., & Müller, P. J. (2003). Reconstruction of SE trade-wind intensity based on sea-surface temperature gradients in the Southeast Atlantic over the last 25 kyr. *Geophysical Research Letters*, *30*(22), 2144. https://doi.org/10.1029/2003GL017557

Kim, J.-H., Rimbu, N., Lorenz, S. J., Lohmann, G., Nam, S.-I., Schouten, S., et al. (2004). North Pacific and North Atlantic sea-surface temperature variability during the Holocene. *Quaternary Science Reviews*, *23*(20), 2141–2154.

Kim, J.-H., Meggers, H., Rimbu, N., Lohmann, G., Freudenthal, T., Müller, P. J., & Schneider, R. R. (2007). Impacts of the North Atlantic gyre circulation on Holocene climate off northwest Africa. *Geology*, *35*(5), 387–390.

Kim, R. A., Lee, K. E., & Bae, S. W. (2015). Sea surface temperature proxies (alkenones, foraminiferal Mg/Ca, and planktonic foraminiferal assemblage) and their implications in the Okinawa Trough. *Progress in Earth and Planetary Science*, *2*(1), 43.

Koutavas, A., & Sachs, J. P. (2008). Northern timing of deglaciation in the eastern equatorial Pacific from alkenone paleothermometry. *Paleoceanography*, *23*, PA4205. https://doi.org/10.1029/2008PA001593

Kudrass, H., Hofmann, A., Doose, H., Emeis, K., & Erlenkeuser, H. (2001). Modulation and amplification of climatic changes in the Northern Hemisphere by the Indian summer monsoon during the past 80 ky. *Geology*, *29*(1), 63–66.

Lamy, F., Rühlemann, C., Hebbeln, D., & Wefer, G. (2002). High-and low-latitude climate control on the position of the southern Peru-Chile Current during the Holocene. *Paleoceanography*, *17*(2), 1028. https://doi.org/10.1029/2001PA000727

Lear, C. H., Rosenthal, Y., & Slowey, N. (2002). Benthic foraminiferal Mg/Ca-paleothermometry: A revised core-top calibration. *Geochimica et Cosmochimica Acta*, *66*(19), 3375–3387.

Leduc, G., Vidal, L., Tachikawa, K., Rostek, F., Sonzogni, C., Beaufort, L., & Bard, E. (2007). Moisture transport across Central America as a positive feedback on abrupt climatic changes. *Nature*, *445*(7130), 908–911.

Leduc, G., Schneider, R., Kim, J.-H., & Lohmann, G. (2010). Holocene and Eemian sea surface temperature trends as revealed by alkenone and Mg/Ca paleothermometry. *Quaternary Science Reviews*, *29*(7), 989–1004.

Lee, K. E., Slowey, N. C., & Herbert, T. D. (2001). Glacial sea surface temperatures in the subtropical North Pacific: A comparison of $U^{K'}_{37}$, $\delta^{18}O$, and foraminiferal assemblage temperature estimates. *Paleoceanography*, *16*(3), 268–279.

Lee, K. E., Kim, J.-H., Wilke, I., Helmke, P., & Schouten, S. (2008). A study of the alkenone, TEX_{86}, and planktonic foraminifera in the Benguela Upwelling System: Implications for past sea surface temperature estimates. *Geochemistry, Geophysics, Geosystems*, *9*, Q10019. https://doi.org/10.1029/2008GC002056

Lee, K. E., Bahk, J. J., & Choi, J. (2008). Alkenone temperature estimates for the East Sea during the last 190,000 years. *Organic Geochemistry*, *39*(6), 741–753.

Leider, A., Hinrichs, K., Mollenhauer, G., & Versteegh, G. (2010). Core-top calibration of the lipid-based $U^{K'}_{37}$ and TEX_{86} temperature proxies on the southern Italian shelf (SW Adriatic Sea, Gulf of Taranto). *Earth and Planetary Science Letters*, *300*, 112–124.

Li, L., Li, Q., Tian, J., Wang, P., Wang, H., & Liu, Z. (2011). A 4-Ma record of thermal evolution in the tropical western Pacific and its implications on climate change. *Earth and Planetary Science Letters*, *309*(1), 10–20.

Liu, Z., & Herbert, T. D. (2004). High-latitude influence on the eastern equatorial Pacific climate in the early Pleistocene epoch. *Nature*, *427*(6976), 720–723.

Locarnini, R. A., Mishonov, A. V., Antonov, J. I., Boyer, T. P., Garcia, H. E., Baranova, O. K., et al. (2013). World Ocean Atlas, 2013, Volume 1: Temperature. In S. Levitus & A. Mishonov (Eds.), *NOAA Atlas NESDIS* (Vol. 73, pp. 1–40). Washington, DC: U.S. Government Printing Office.

Lückge, A., Mohtadi, M., Rühlemann, C., Scheeder, G., Vink, A., Reinhardt, L., & Wiedicke, M. (2009). Monsoon versus ocean circulation controls on paleoenvironmental conditions off southern Sumatra during the past 300,000 years. *Paleoceanography*, *24*, PA1208. https://doi.org/10.1029/2008PA001627

Madureira, L. A., Conte, M. H., & Eglinton, G. (1995). Early diagenesis of lipid biomarker compounds in North Atlantic sediments. *Paleoceanography*, *10*(3), 627–642.

Marchal, O., Cacho, I., Stocker, T. F., Grimalt, J. O., Calvo, E., Martrat, B., et al. (2002). Apparent long-term cooling of the sea surface in the Northeast Atlantic and Mediterranean during the holocene. *Quaternary Science Reviews*, *21*(4), 455–483.

Marlowe, I., Brassell, S., Eglinton, G., & Green, J. (1984). Long chain unsaturated ketones and esters in living algae and marine sediments. *Organic Geochemistry*, *6*, 135–141.

Marlowe, I., Brassell, S., Eglinton, G., & Green, J. (1990). Long-chain alkenones and alkyl alkenoates and the fossil coccolith record of marine sediments. *Chemical Geology*, *88*(3-4), 349–375.

Martrat, B., Grimalt, J. O., Shackleton, N. J., de Abreu, L., Hutterli, M. A., & Stocker, T. F. (2007). Four climate cycles of recurring deep and surface water destabilizations on the Iberian margin. *Science*, *317*(5837), 502–507.

Max, L., Riethdorf, J.-R., Tiedemann, R., Smirnova, M., Lembke-Jene, L., Fahl, K., et al. (2012). Sea surface temperature variability and sea-ice extent in the subarctic northwest Pacific during the past 15,000 years. *Paleoceanography*, *27*, PA3213. https://doi.org/10.1029/2012PA002292

McCaffrey, M. A., Farrington, J. W., & Repeta, D. J. (1990). The organic geochemistry of Peru margin surface sediments: I. A comparison of the C_{37} alkenone and historical El Niño records. *Geochimica et Cosmochimica Acta*, *54*(6), 1671–1682.

Mohtadi, M., Steinke, S., Lückge, A., Groeneveld, J., & Hathorne, E. (2010). Glacial to Holocene surface hydrography of the tropical eastern Indian Ocean. *Earth and Planetary Science Letters*, *292*(1–2), 89–97.

Mohtadi, M., Oppo, D. W., Lückge, A., DePol-Holz, R., Steinke, S., Groeneveld, J., et al. (2011). Reconstructing the thermal structure of the upper ocean: Insights from planktic foraminifera shell chemistry and alkenones in modern sediments of the tropical eastern Indian Ocean. *Paleoceanography*, *26*, PA3219. https://doi.org/10.1029/2011PA002132

Mohtadi, M., Prange, M., Oppo, D. W., De Pol-Holz, R., Merkel, U., Zhang, X., et al. (2014). North Atlantic forcing of tropical Indian Ocean climate. *Nature*, *509*(7498), 76–80.

Mollenhauer, G., Eglinton, T., Ohkouchi, N., Schneider, R., Müller, P., Grootes, P., & Rullkötter, J. (2003). Asynchronous alkenone and foraminifera records from the Benguela Upwelling System. *Geochimica et Cosmochimica Acta*, *67*(12), 2157–2171.

Müller, P., Kirst, G., Ruhland, G., Von Storch, I., & Rosell-Melé, A. (1998). Calibration of the alkenone paleotemperature index $U^{K'}_{37}$ based on core-tops from the eastern South Atlantic and the global ocean (60N–60°S). *Geochimica et Cosmochimica Acta*, *62*(10), 1757–1772.

Müller, P. J., & Fischer, G. (2001). A 4-year sediment trap record of alkenones from the filamentous upwelling region off Cape Blanc, NW Africa and a comparison with distributions in underlying sediments. *Deep Sea Research Part I: Oceanographic Research Papers*, *48*(8), 1877–1903.

O'Brien, C. L., Foster, G. L., Martínez-Botí, M. A., Abell, R., Rae, J. W., & Pancost, R. D. (2014). High sea surface temperatures in tropical warm pools during the Pliocene. *Nature Geoscience*, *7*(8), 606–611.

Ohkouchi, N., Kawamura, K., Kawahata, H., & Okada, H. (1999). Depth ranges of alkenone production in the central Pacific Ocean. *Global Biogeochemical Cycles*, *13*(2), 695–704.

Ostertag-Henning, C., & Stax, R. (2000). Data report: Carbonate records from sites 1012, 1013, 1017, and 1019 and alkenone-based sea-surface temperatures from site 1017, *167*, pp. 297–302.

Pahnke, K., & Sachs, J. P. (2006). Sea surface temperatures of southern midlatitudes 0–160 kyr BP. *Paleoceanography*, *21*, PA2003. https://doi.org/10.1029/2005PA001191

Pahnke, K., Sachs, J. P., Keigwin, L., Timmermann, A., & Xie, S.-P. (2007). Eastern tropical Pacific hydrologic changes during the past 27,000 years from D/H ratios in alkenones. *Paleoceanography*, *22*, PA4214. https://doi.org/10.1029/2007PA001468

Pailler, D., & Bard, E. (2002). High frequency palaeoceanographic changes during the past 140 000 yr recorded by the organic matter in sediments of the Iberian Margin. *Palaeogeography, Palaeoclimatology, Palaeoecology*, *181*(4), 431–452.

Palmer, M., & Pearson, P. N. (2003). A 23,000-year record of surface water pH and pCO_2 in the western equatorial Pacific Ocean. *Science*, *300*(5618), 480–482.

Pearson, P., van Dongen, B. E., Nicholas, C. J., Pancost, R. D., Schouten, S., Singano, J. M., & Wade, B. S. (2007). Stable warm tropical climate through the Eocene Epoch. *Geology*, *35*(3), 211–214.

Pelejero, C., & Calvo, E. (2003). The upper end of the $U^{K'}_{37}$ temperature calibration revisited. *Geochemistry, Geophysics, Geosystems*, *4*, 1014. https://doi.org/10.1029/2002GC000431

Pelejero, C., & Grimalt, J. O. (1997). The correlation between the $U^{K'}_{37}$ index and sea surface temperatures in the warm boundary: The South China Sea. *Geochimica et Cosmochimica Acta*, *61*(22), 4789–4797.

Pelejero, C., Grimalt, J. O., Heilig, S., Kienast, M., & Wang, L. (1999). High-resolution U^{K}_{37} temperature reconstructions in the South China Sea over the past 220 kyr. *Paleoceanography*, *14*(2), 224–231.

Peyron, O., Guiot, J., Cheddadi, R., Tarasov, P., Reille, M., de Beaulieu, J.-L., et al. (1998). Climatic reconstruction in Europe for 18,000 yr BP from pollen data. *Quaternary research*, *49*(2), 183–196.

Praetorius, S., Mix, A., Walczak, M., Wolhowe, M., Addison, J., & Prahl, F. (2015). North Pacific deglacial hypoxic events linked to abrupt ocean warming. *Nature*, *527*(7578), 362–366.

Prahl, F., & Wakeham, S. (1987). Calibration of unsaturation patterns in long-chain ketone compositions for palaeotemperature assessment. *Nature*, *330*, 367–369.

Prahl, F., Muehlhausen, L., & Zahnle, D. (1988). Further evaluation of long-chain alkenones as indicators of paleoceanographic conditions. *Geochimica et Cosmochimica Acta*, *52*(9), 2303–2310.

Prahl, F., De Lange, G., Lyle, M., & Sparrow, M. (1989). Post-depositional stability of long-chain alkenones under contrasting redox conditions. *Nature*, *341*(6241), 434–437.

Prahl, F., Muehlhausen, L., & Lyle, M. (1989). An organic geochemical assessment of oceanographic conditions at MANOP Site C over the past 26,000 years. *Paleoceanography*, *4*(5), 495–510.

Prahl, F., Collier, R., Dymond, J., Lyle, M., & Sparrow, M. (1993). A biomarker perspective on prymnesiophyte productivity in the northeast Pacific Ocean. *Deep Sea Research Part I: Oceanographic Research Papers*, *40*(10), 2061–2076.

Prahl, F., Herbert, T., Brassell, S., Ohkouchi, N., Pagani, M., Repeta, D., et al. (2000). Status of alkenone paleothermometer calibration: Report from Working Group 3. *Geochemistry, Geophysics, Geosystems*, *1*(11), 1034.

Prahl, F., Sparrow, M., & Wolfe, G. (2003). Physiological impacts on alkenone paleothermometry. *Paleoceanography*, *18*(2), 1025. https://doi.org/10.1029/2002PA000803

Prahl, F., Rontani, J., Zabeti, N., Walinsky, S., & Sparrow, M. (2010). Systematic pattern in $U^{K'}_{3}$ 7-temperature residuals for surface sediments from high latitude and other oceanographic settings. *Geochimica et Cosmochimica Acta*, *74*(1), 131–143.

Prahl, F. G., Mix, A. C., & Sparrow, M. A. (2006). Alkenone paleothermometry: Biological lessons from marine sediment records off western South America. *Geochimica et Cosmochimica Acta*, *70*(1), 101–117.

Raffi, I., Backman, J., Fornaciari, E., Pälike, H., Rio, D., Lourens, L., & Hilgen, F. (2006). A review of calcareous nannofossil astrobiochronology encompassing the past 25 million years. *Quaternary Science Reviews*, *25*(23), 3113–3137.

Ravelo, A. C., Lawrence, K. T., Fedorov, A., & Ford, H. L. (2014). Comment on "A 12-million-year temperature history of the tropical Pacific Ocean". *Science*, *346*(6216), 1467–1467.

Regenberg, M., Regenberg, A., Garbe-Schönberg, D., & Lea, D. W. (2014). Global dissolution effects on planktonic foraminiferal Mg/Ca ratios controlled by the calcite-saturation state of bottom waters. *Paleoceanography*, *29*, 127–142. https://doi.org/10.1002/2013PA002492

Reimer, P. J., Bard, E., Bayliss, A., Beck, J. W., Blackwell, P. G., Ramsey, C. B., et al. (2013). IntCal13 and Marine 13 radiocarbon age calibration curves 0–50,000 years cal BP. *Radiocarbon*, *55*(4), 1869–1887.

Rein, B., Lückge, A., Reinhardt, L., Sirocko, F., Wolf, A., & Dullo, W.-C. (2005). El Niño variability off Peru during the last 20,000 years. *Paleoceanography*, *20*, PA4003. https://doi.org/10.1029/2004PA001099

Richey, J. N., & Tierney, J. E. (2016). GDGT and alkenone flux in the northern Gulf of Mexico: Implications for the TEX_{86} and $U^{K'}_{37}$ paleothermometers. *Paleoceanography*, *31*, 1547–1561. https://doi.org/10.1002/2016PA003032

Rippert, N., Baumann, K.-H., & Pätzold, J. (2015). Thermocline fluctuations in the western tropical Indian Ocean during the past 35 ka. *Journal of Quaternary Science*, *30*(3), 201–210.

Rodrigo-Gámiz, M., Rampen, S., de Haas, H., Baas, M., Schouten, S., & Sinninghe Damsté, J. (2015). Constraints on the applicability of the organic temperature proxies $U^{K'}_{37}$, TEX_{86} and LDI in the subpolar region around Iceland. *Biogeosciences*, *12*(22), 6573–6590.

Rodrigues, T., Grimalt, J. O., Abrantes, F. G., Flores, J. A., & Lebreiro, S. M. (2009). Holocene interdependences of changes in sea surface temperature, productivity, and fluvial inputs in the Iberian continental shelf (Tagus mud patch). *Geochemistry, Geophysics, Geosystems*, *10*, Q07U06. https://doi.org/10.1029/2008GC002367

Rodrigues, T., Grimalt, J. O., Abrantes, F., Naughton, F., & Flores, J.-A. (2010). The last glacial–interglacial transition (LGIT) in the western mid-latitudes of the North Atlantic: Abrupt sea surface temperature change and sea level implications. *Quaternary Science Reviews*, *29*(15), 1853–1862.

Romahn, S., Mackensen, A., Groeneveld, J., & Pätzold, J. (2014). Deglacial intermediate water reorganization: New evidence from the Indian Ocean. *Climate of the Past*, *10*(1), 293–303.

Romero, O. E., Kim, J.-H., & Donner, B. (2008). Submillennial-to-millennial variability of diatom production off Mauritania, NW Africa, during the last glacial cycle. *Paleoceanography*, *23*, PA3218. https://doi.org/10.1029/2008PA001601

Rosell-Melé, A. (1998). Interhemispheric appraisal of the value of alkenone indices as temperature and salinity proxies in high-latitude locations. *Paleoceanography*, *13*(6), 694–703.

Rosell-Melé, A., & Prahl, F. G. (2013). Seasonality of $U^{K'}_{37}$ temperature estimates as inferred from sediment trap data. *Quaternary Science Reviews*, *72*, 128–136.

Rosell-Melé, A., Eglinton, G., Pflaumann, U., & Sarnthein, M. (1995). Atlantic core-top calibration of the U^{K}_{37} index as a sea-surface palaeotemperature indicator. *Geochimica et Cosmochimica Acta*, *59*(15), 3099–3107.

Rosell-Mele, A., Comes, P., Müller, P. J., & Ziveri, P. (2000). Alkenone fluxes and anomalous $U^{K'}_{37}$ values during 1989–1990 in the Northeast Atlantic (48°N 21°W). *Marine Chemistry*, *71*(3), 251–264.

Rosell-Melé, A., Bard, E., Emeis, K.-C., Grieger, B., Hewitt, C., Müller, P. J., & Schneider, R. R. (2004). Sea surface temperature anomalies in the oceans at the LGM estimated from the alkenone-$U^{K'}_{37}$ index: Comparison with GCMs. *Geophysical Research Letters*, *31*, L03208. https://doi.org/10.1029/2003GL018151

Rühlemann, C., & Butzin, M. (2006). Alkenone temperature anomalies in the Brazil-Malvinas Confluence area caused by lateral advection of suspended particulate material. *Geochemistry, Geophysics, Geosystems*, *7*, Q10015. https://doi.org/10.1029/2006GC001251

Rühlemann, C., Mulitza, S., Müller, P. J., Wefer, G., & Zahn, R. (1999). Warming of the tropical Atlantic Ocean and slowdown of thermohaline circulation during the last deglaciation. *Nature*, *402*(6761), 511–514.

Sachs, J. P. (2007). Cooling of Northwest Atlantic slope waters during the Holocene. *Geophysical Research Letters*, *34*, L03609. https://doi.org/10.1029/2006GL028495

Samtleben, C. (1980). Die evolution der coccolithophoriden-Gattung Gephyrocapsa nach Befunden im Atlantik. *Palä,ontologische Zeitschrift*, *54*(1), 91–127.

Saraswat, R., Lea, D. W., Nigam, R., Mackensen, A., & Naik, D. K. (2013). Deglaciation in the tropical Indian Ocean driven by interplay between the regional monsoon and global teleconnections. *Earth and Planetary Science Letters*, *375*, 166–175.

Sawada, K., & Handa, N. (1998). Variability of the path of the Kuroshio ocean current over the past 25,000 years. *Nature*, *392*(6676), 592–595.

Sawada, K., Handa, N., Shiraiwa, Y., Danbara, A., & Montani, S. (1996). Long-chain alkenones and alkyl alkenoates in the coastal and pelagic sediments of the northwest North Pacific, with special reference to the reconstruction of Emiliania huxleyi and Gephyrocapsa oceanica ratios. *Organic Geochemistry*, *24*(8), 751–764.

Schefuß, E., Schouten, S., & Schneider, R. R. (2005). Climatic controls on central African hydrology during the past 20,000 years. *Nature*, *437*(7061), 1003–1006.

Schmittner, A., Urban, N. M., Shakun, J. D., Mahowald, N. M., Clark, P. U., Bartlein, P. J., et al. (2011). Climate sensitivity estimated from temperature reconstructions of the Last Glacial Maximum. *Science*, *334*(6061), 1385–1388.

Schulte, S., & Müller, P. J. (2001). Variations of sea surface temperature and primary productivity during Heinrich and Dansgaard-Oeschger events in the northeastern Arabian Sea. *Geo-Marine Letters*, *21*(3), 168–175.

Schulz, H., Emeis, K.-C., Erlenkeuser, H., von Rad, U., & Rolf, C. (2002). The Toba volcanic event and interstadial/stadial climates at the marine isotopic stage 5 to 4 transition in the northern Indian Ocean. *Quaternary Research*, *57*(1), 22–31.

Seki, O., Kawamura, K., Ikehara, M., Nakatsuka, T., & Oba, T. (2004). Variation of alkenone sea surface temperature in the Sea of Okhotsk over the last 85 kyrs. *Organic Geochemistry*, *35*(3), 347–354.

Seki, O., Nakatsuka, T., Kawamura, K., Saitoh, S.-I., & Wakatsuchi, M. (2007). Time-series sediment trap record of alkenones from the western Sea of Okhotsk. *Marine Chemistry*, *104*(3), 253–265.

Sepúlveda, J., Pantoja, S., Hughen, K. A., Bertrand, S., Figueroa, D., León, T., et al. (2009). Late Holocene sea-surface temperature and precipitation variability in northern Patagonia, Chile (Jacaf Fjord, 44°S). *Quaternary Research*, *72*(3), 400–409.

Shakun, J. D., & Carlson, A. E. (2010). A global perspective on Last Glacial Maximum to Holocene climate change. *Quaternary Science Reviews*, *29*(15), 1801–1816.

Shintani, T., Yamamoto, M., & Chen, M.-T. (2008). Slow warming of the northern South China Sea during the last deglaciation, terrestrial. *Atmospheric & Oceanic Sciences*, *19*(4), 341–346.

Shintani, T., Yamamoto, M., & Chen, M.-T. (2011). Paleoenvironmental changes in the northern South China Sea over the past 28,000 years: A study of TEX_{86}-derived sea surface temperatures and terrestrial biomarkers. *Journal of Asian Earth Sciences*, *40*(6), 1221–1229.

Sicre, M.-A., Bard, E., Ezat, U., & Rostek, F. (2002). Alkenone distributions in the North Atlantic and Nordic sea surface waters. *Geochemistry, Geophysics, Geosystems*, *3*(2), 1–13. https://doi.org/10.1029/2001GC000159

Sikes, E., Farrington, J. t., & Keigwin, L. (1991). Use of the alkenone unsaturation ratio U^{K}_{37} to determine past sea surface temperatures: Core-top SST calibrations and methodology considerations. *Earth and Planetary Science Letters*, *104*(1), 36–47.

Sikes, E. L., & Keigwin, L. D. (1994). Equatorial Atlantic sea surface temperature for the last 30 kyr: A comparison of $U^{K'}_{37}$, $\delta^{18}O$ and foraminiferal assemblage temperature estimates. *Paleoceanography*, *9*(1), 31–45.

Sikes, E. L., & Keigwin, L. D. (1996). A reexamination of northeast Atlantic sea surface temperature and salinity over the last 16 kyr. *Paleoceanography*, *11*(3), 327–342.

Sikes, E. L., & Volkman, J. K. (1993). Calibration of alkenone unsaturation ratios (Uk'37) for paleotemperature estimation in cold polar waters. *Geochimica et Cosmochimica Acta*, *57*(8), 1883–1889.

Sikes, E. L., Volkman, J. K., Robertson, L. G., & Pichon, J.-J. (1997). Alkenones and alkenes in surface waters and sediments of the Southern Ocean: Implications for paleotemperature estimation in polar regions. *Geochimica et Cosmochimica Acta*, *61*(7), 1495–1505.

Sikes, E. L., O'Leary, T., Nodder, S. D., & Volkman, J. K. (2005). Alkenone temperature records and biomarker flux at the subtropical front on the Chatham Rise. *SW Pacific Ocean Deep Sea Research Part I*, *52*(5), 721–748.

Sikes, E. L., Howard, W. R., Samson, C. R., Mahan, T. S., Robertson, L. G., & Volkman, J. K. (2009). Southern Ocean seasonal temperature and Subtropical Front movement on the South Tasman Rise in the late Quaternary. *Paleoceanography*, *24*, PA2201. https://doi.org/10.1029/2008PA001659

Sonzogni, C., Bard, E., Rostek, F., Dollfus, D., Rosell-Melé, A., & Eglinton, G. (1997). Temperature and salinity effects on alkenone ratios measured in surface sediments from the Indian Ocean. *Quaternary Research*, *47*(3), 344–355.

Sonzogni, C., Bard, E., & Rostek, F. (1998). Tropical sea-surface temperatures during the last glacial period: A view based on alkenones in Indian Ocean sediments. *Quaternary Science Reviews*, *17*(12), 1185–1201.

Sperling, M., Schmiedl, G., Hemleben, C., Emeis, K., Erlenkeuser, H., & Grootes, P. (2003). Black Sea impact on the formation of eastern Mediterranean sapropel S1? Evidence from the Marmara Sea. *Palaeogeography, Palaeoclimatology, Palaeoecology*, *190*, 9–21.

Steiger, N., & Hakim, G. (2016). Multi-timescale data assimilation for atmosphere–ocean state estimates. *Climate of the Past*, *12*(6), 1375–1388.

Stott, L., Timmermann, A., & Thunell, R. (2007). Southern hemisphere and deep-sea warming led deglacial atmospheric CO_2 rise and tropical warming. *Science*, *318*(5849), 435–438.

Tao, S., Xing, L., Luo, X., Wei, H., Liu, Y., & Zhao, M. (2012). Alkenone distribution in surface sediments of the southern yellow sea and implications for the $u^{K'}_{37}$ thermometer. *Geo-Marine Letters*, *32*(1), 61–71.

Ternois, Y., Sicre, M.-A., Boireau, A., Marty, J.-C., & Miquel, J.-C. (1996). Production pattern of alkenones in the Mediterranean Sea. *Geophysical Research Letters*, *23*(22), 3171–3174.

Ternois, Y., Sicre, M.-A., Boireau, A., Conte, M., & Eglinton, G. (1997). Evaluation of long-chain alkenones as paleo-temperature indicators in the Mediterranean Sea. *Deep Sea Research Part I: Oceanographic Research Papers*, *44*(2), 271–286.

Ternois, Y., Kawamura, K., Ohkouchi, N., & Keigwin, L. (2000). Alkenone sea surface temperature in the Okhotsk Sea for the last 15 kyr. *Geochemical Journal*, *34*(4), 283–293.

Thierstein, H., Geitzenauer, K., Molfino, B., & Shackleton, N. (1977). Global synchroneity of late Quaternary coccolith datum levels: Validation by oxygen isotopes. *Geology*, *5*(7), 400–404.

Thomsen, C., Schulz-Bull, D. E., Petrick, G., & Duinker, J. C. (1998). Seasonal variability of the long-chain alkenone flux and the effect on the $U^{K'}_{37}$-index in the Norwegian Sea. *Organic Geochemistry*, *28*(5), 311–323.

Tierney, J. E., & Tingley, M. P. (2014). A Bayesian, spatially-varying calibration model for the TEX_{86} proxy. *Geochimica et Cosmochimica Acta*, *127*, 83–106.

Tierney, J. E., & Tingley, M. P. (2015). A TEX_{86} surface sediment database and extended Bayesian calibration. *Scientific Data*, *2*(150029).

Tierney, J. E., Pausata, F. S., & deMenocal, P. B. (2016). Deglacial Indian monsoon failure and North Atlantic stadials linked by Indian Ocean surface cooling. *Nature Geoscience*, *9*(1), 46–50.

Tingley, M. P., Craigmile, P. F., Haran, M., Li, B., Mannshardt, E., & Rajaratnam, B. (2012). Piecing together the past: Statistical insights into paleoclimatic reconstructions. *Quaternary Science Reviews*, *35*, 1–22.

Volkman, J. K., Eglinton, G., Corner, E. D., & Forsberg, T. (1980). Long-chain alkenes and alkenones in the marine coccolithophorid Emiliania huxleyi. *Phytochemistry*, *19*(12), 2619–2622.

Volkman, J. K., Barrerr, S. M., Blackburn, S. I., & Sikes, E. L. (1995). Alkenones in Gephyrocapsa oceanica: Implications for studies of paleoclimate. *Geochimica et Cosmochimica Acta*, *59*(3), 513–520.

Waelbroeck, C., Paul, A., Kucera, M., Rosell-Melé, A., Weinelt, M., Schneider, R., et al. (2009). Constraints on the magnitude and patterns of ocean cooling at the Last Glacial Maximum. *Nature Geoscience*, *2*(2), 127–132.

Weldeab, S., Schneider, R. R., & Müller, P. (2007). Comparison of Mg/Ca-and alkenone-based sea surface temperature estimates in the fresh water–influenced Gulf of Guinea, eastern equatorial Atlantic. *Geochemistry, Geophysics, Geosystems*, *8*, Q05P22. https://doi.org/10.1029/2006GC001360

Xu, J., Holbourn, A., Kuhnt, W., Jian, Z., & Kawamura, H. (2008). Changes in the thermocline structure of the Indonesian outflow during Terminations I and II. *Earth and Planetary Science Letters*, *273*(1), 152–162.

Xu, J., Kuhnt, W., Holbourn, A., Regenberg, M., & Andersen, N. (2010). Indo-Pacific Warm Pool variability during the Holocene and Last Glacial Maximum. *Paleoceanography*, *25*, PA4230. https://doi.org/10.1029/2010PA001934

Yamamoto, M., Sai, H., Chen, M.-T., & Zhao, M. (2013). The East Asian winter monsoon variability in response to precession during the past 150,000 yr. *Climate of the Past*, *9*(6), 2777–2788.

Zachos, J. C., Stott, L. D., & Lohmann, K. C. (1994). Evolution of early Cenozoic marine temperatures. *Paleoceanography*, *9*(2), 353–387.

Zhang, Y. G., Pagani, M., & Liu, Z. (2014). A 12-million-year temperature history of the tropical Pacific Ocean. *Science*, *344*(6179), 84–87.

Zhao, M., Beveridge, N., Shackleton, N., Sarnthein, M., & Eglinton, G. (1995). Molecular stratigraphy of cores off northwest Africa: Sea surface temperature history over the last 80 ka. *Paleoceanography*, *10*(3), 661–675.

Zhao, M., Huang, C.-Y., Wang, C.-C., & Wei, G. (2006). A millennial-scale $U^{K'}_{37}$ sea-surface temperature record from the South China Sea (8°N) over the last 150 kyr: Monsoon and sea-level influence. *Palaeogeography, Palaeoclimatology, Palaeoecology*, *236*(1), 39–55.